Single dish calibration

Carsten Kramer, IRAM Granada

10th IRAM mm Interferometer School
1-5 October 2018

Single dish calibration: Motivation

Motivation:

The aim of astronomical observations is often to obtain physical parameters of the emitting regions, like temperatures, densities, column densities, masses, polarisation (angle, degree), time variability (periodicity), etc..

To derive these quantities from the detected data, the data have to be calibrated. This means for example to translate the observed counts into intensities.

Many of the properties of the receiving system have to be known, as accurately as possible, as they influence the observed data. For example, the telescope has a finite angular resolution, as the spectrometers have a finite frequency resolution.

Here, we will speak about electro-magnetic waves in the mm-regime, detected with single-dish radio telescopes.

IRC+10216: An evolved star

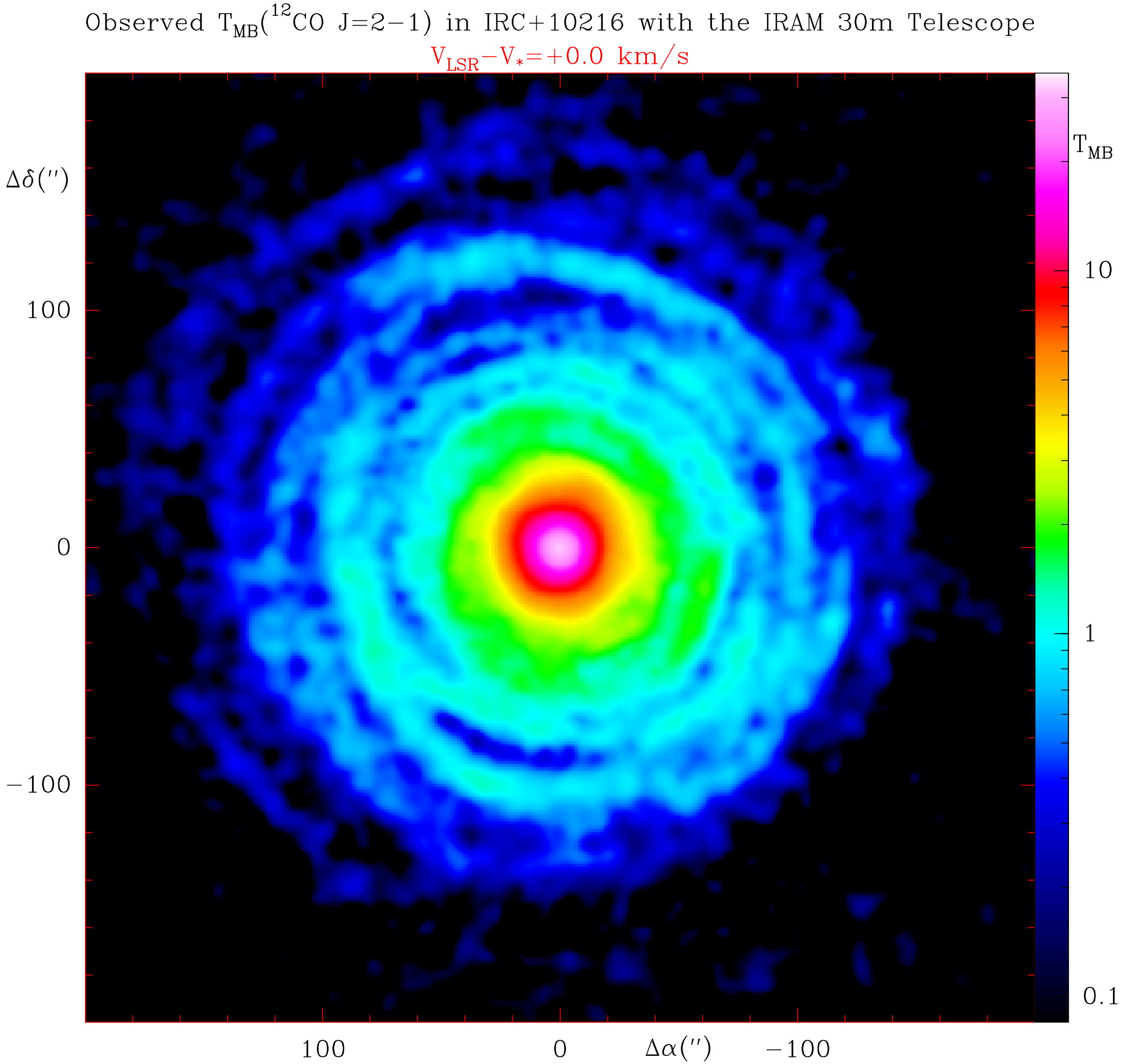

- Mass loss of AGB stars via stellar ejecta enrich the ISM and largely control the chemical evolution of galaxies
- Here, CO emission of the shells of carbon-rich AGB star IRC+10216 at 120pc distance
- Envelope is nearly spherical, expanding at 14.5 km/s.
- The resolution of 11″ corresponds to an expansion time of 500 yr. The map shows the mass loss history of the last 8000 yr. The typical shell separation is 800-1000 yr.
- A companion star with a period of 800 yr would explain all key features.
- Cernicharo et al. 2015, A&A, 575, A91
- IRC+10216 exhibits a very rich chemistry. Nearly 50% of the known interstellar species have been found here.

Detection of methyl silane CH_3SiH_3 in IRC+10216

- The detection of organo-silicon molecule CH_3SiH_3 may help in understanding of silicon-carbon chemistries in the inner envelope of AGB stars, and the formation of SiC grains from gas-phase Si_nC_m.
- Ten rotational transitions detected with the IRAM 30m telescope between 80 and 350 GHz:
  J=4-3 to J=16-15
- Blue: Observed spectrum

  Green: Modelled CH_3SiH_3 spectrum
  Red arrows indicate K-ladder.
- Cernicharo, Agundez et al. 2017 (A&A, 606, 5)

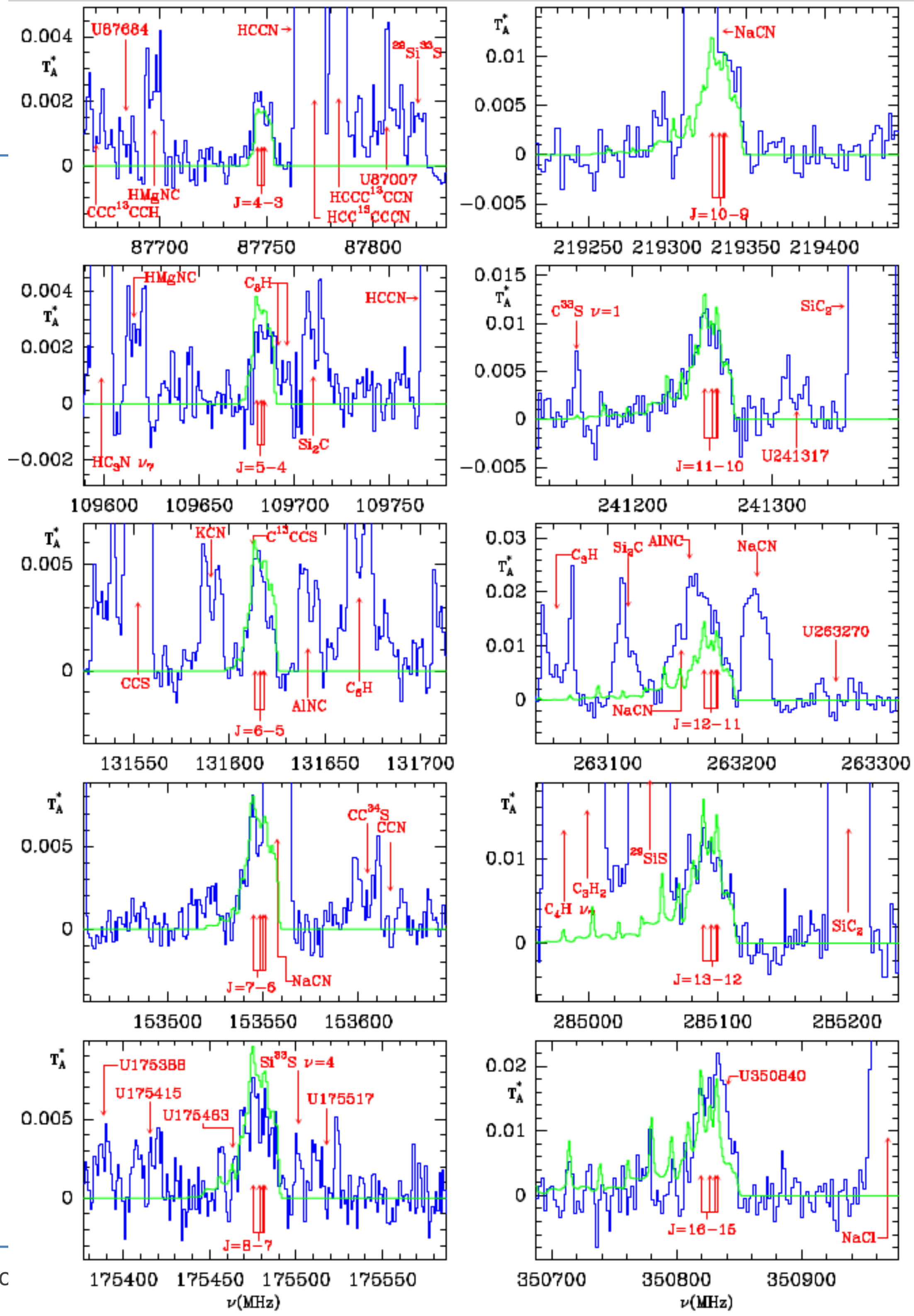

IRC+10216

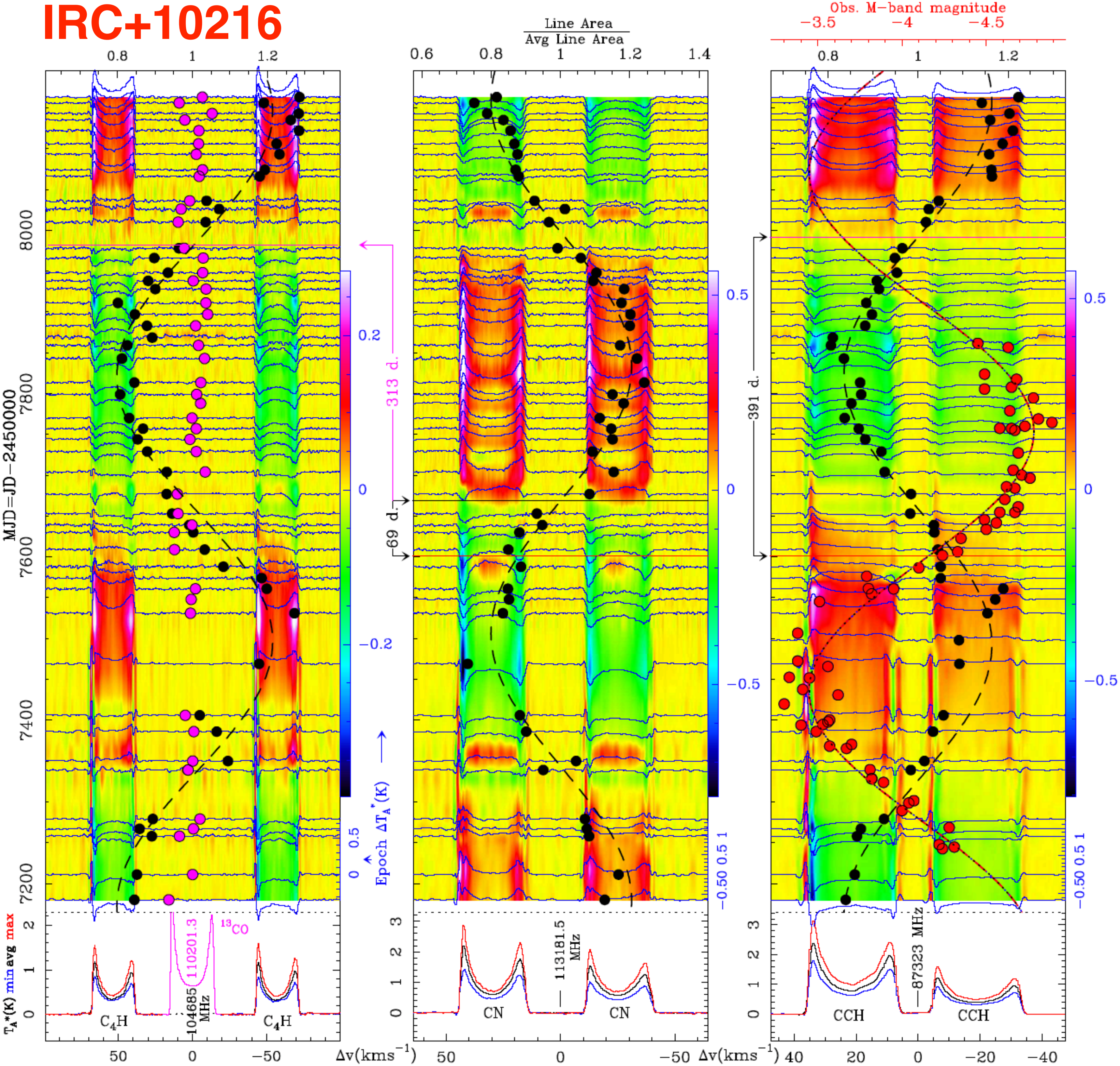

iram
Institut de Radioastronomie Millimétrique

Periodic time variability of C_4H, C_2H, CN in IRC+10216

Period = 635 days

(Pardo et al. 2018, A&A)

Single dish calibration: Contents & Literature

Contents:

1. Telescope: IRAM 30m telescope and others
2. Atmosphere
3. Point spread function of the telescope: the beam or antenna diagram
4. Heterodyne Receivers: temperature, sideband gain ratio
5. Antenna temperatures and “Chopperwheel” calibration
6. Telescope efficiencies: aperture, main beam, forward
7. Stability and observing switching modes

Literature:

- Lectures by ClemensThum, Pierre Hily-Blant, Bertrand Lefloch, Michael Bremer at previous IRAM summerschools in Spain and France
- **Tom Wilson and Susanne Huettemeister: Tools of Radio Astronomy**
- Jaap Baars 2007: The paraboloidal reflector antenna in radio astronomy
- Albert Greve & Michael Bremer 2010: Thermal design and thermal behaviour of radio telescopes and their enclosures

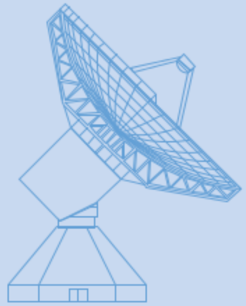

30 meter telescope

Location	Pico Veleta, Sierra Nevada, Spain
Altitude	2850 meters
Longitude / Latitude	03:23:33.7 W / 37:03:58.3 N
Number of antennas	1
Antenna diameter	30 meters
Antenna weight	800 tons
Antenna mount	Alt-azimuth, steel on concrete pedestal
Dish panels	420 aluminium panels on honeycomb back-structure
Secondary mirror diameter	2 meters
Surface precision	55 microns
Tracking precision during observations	< 1/3600° (less than one arcsecond)
Frequencies / wavelengths	80 to 370 GHz / 3 to 0.8 millimeters

30m telescope: principal components

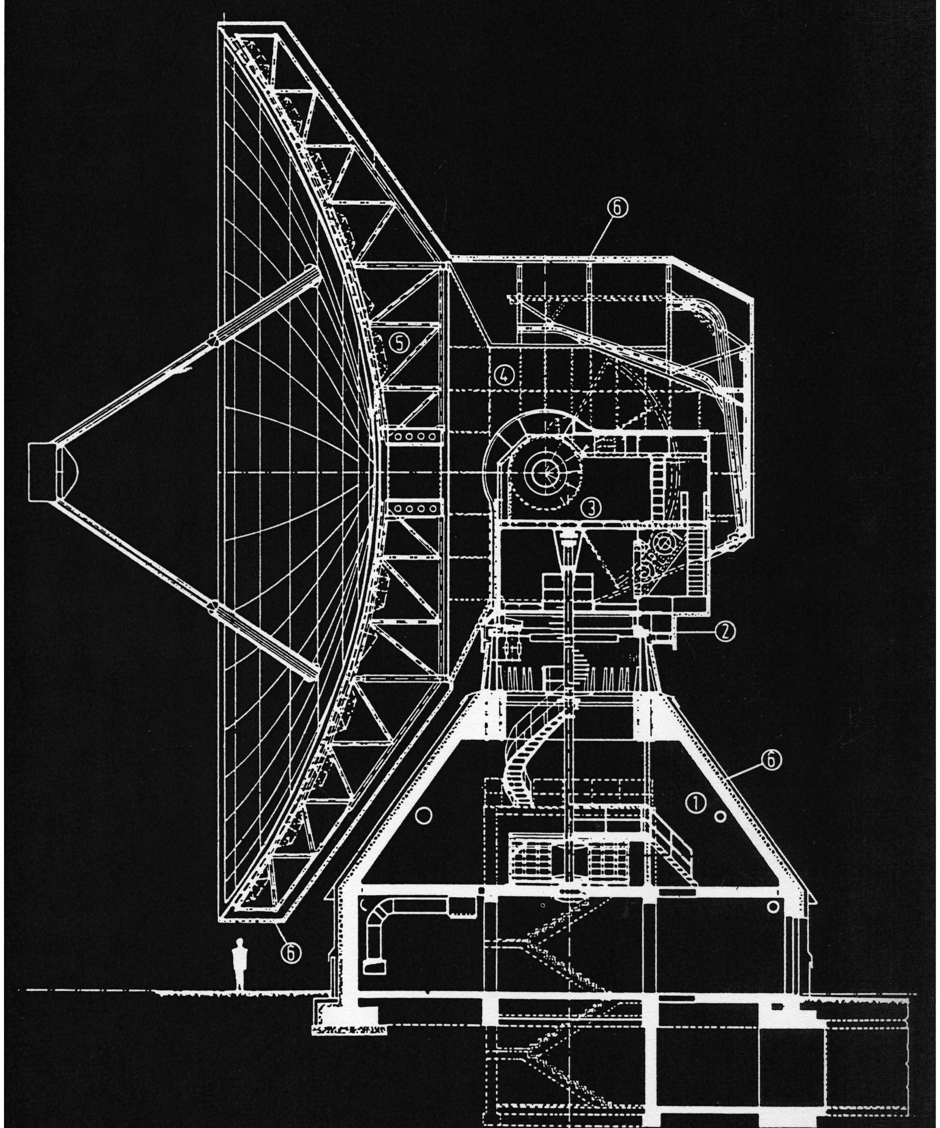

Schéma du télescope de 30-m : 1) Piédestal 2) Roulement en azimuth 3) Cabine de récepteurs 4) Travée d'élévation 5) Structure de support du réflecteur 6) Isolation thermique.

Schematisches Diagramm des 30-m Teleskops : 1) Sockel 2) Azimuth-Lager 3) Empfänger-Kabine 4) Elevationsjoch 5) Reflektor-Tragestruktur 6) Thermische Isolierung.

1. pedestal
2. azimuth bearing
3. elevation axis
4. Nasmyth cabin with frontends & optics
5. backstructure
   steel space frame
   temperature controlled
6. surface of primary mirror
   420 aluminum honeycomb panels
   thermal insulation, deicing
7. quadrupod, subreflector, wobbler

30m telescope: Signal path

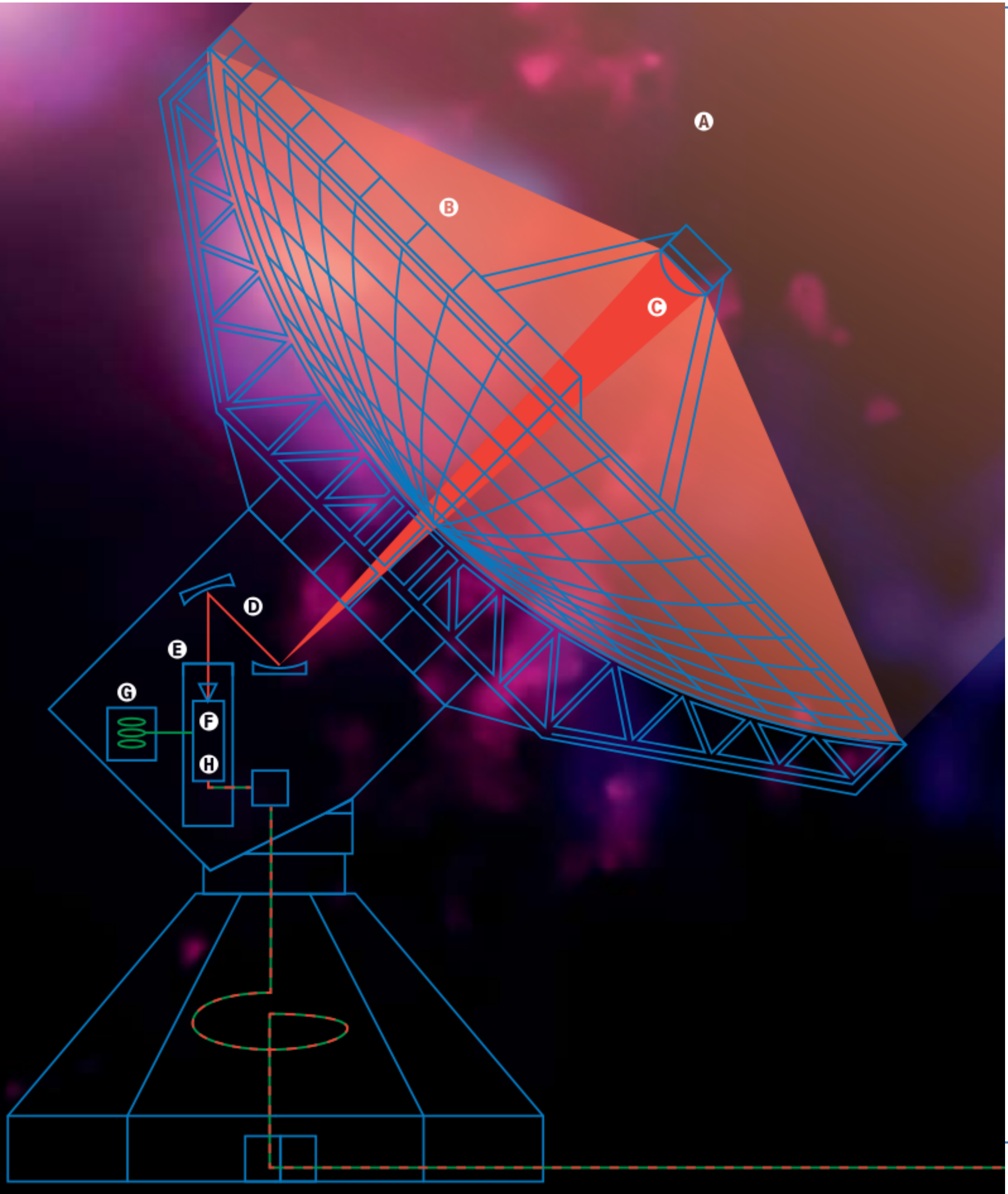

A/ Radiofrequency, RF, Signal

B/ Paraboloic primary mirror

C/ Hyperbolic secondary mirror
Quadrupod support

D/ Flat tertiary mirror M3

E/ Nasmyth optics M3, M4, ...

F/ Heterodyne Receiver
Local oscillator
Mixer
Intermediate frequency, IF

IF-Transport through cable spiral

Spectrometers / Backends

Radio telescope: Alternative designs: pro & cons

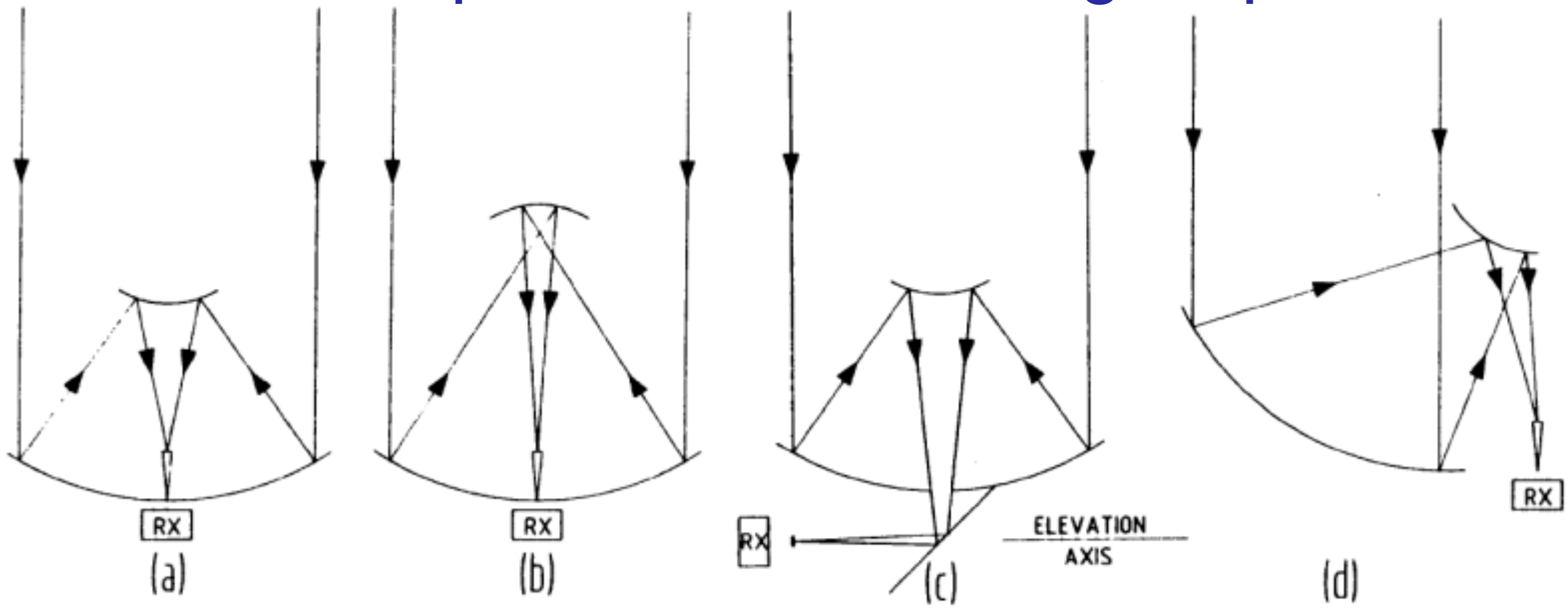

Fig. 7.6 The geometry of (**a**) Cassegrain, (**b**) Gregory, (**c**) Nasmyth and (**d**) offset Cassegrain systems

From Tools of Radioastronomy, Wilson & Huettemeister

Parabolic primary dish, but different secondary mirrors and positions of the receivers:
+ Cassegrain: hyperbolic, convex subreflector (e.g. APEX)
+ Gregory: elliptical, concave subreflector behind the prime focus (e.g. Effelsberg 100m)
+ Nasmyth: hyperbolic subreflector and flat tertiary mirror (e.g. IRAM 30m, 12m APEX, SMT/HHT)
+ Offset Cassegrain: "half" parabolic and hyperbolic subreflector (e.g. 100m GBT, 10m SPT)

Advantages of the different optical configurations:
+ Secondary focus:
  5-10 times larger f/D ratios, less sensitive to lateral focus offsets, larger fields-of-view allowing for array receivers, spillover towards cold sky not warm ground
+ Nasmyth system: receivers are not tilted with elevation, more space
+ Offset Cassegrain: less blockage by subreflector and support structure, less standing waves



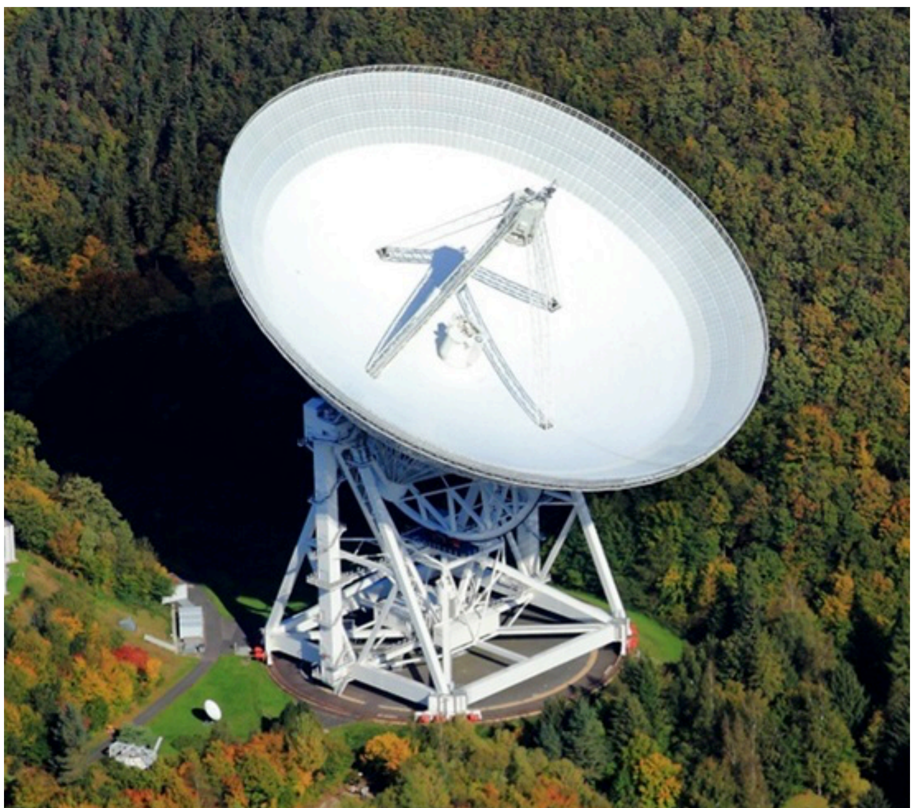


Radio telescopes: Nasmyth optics of the 30m telescope

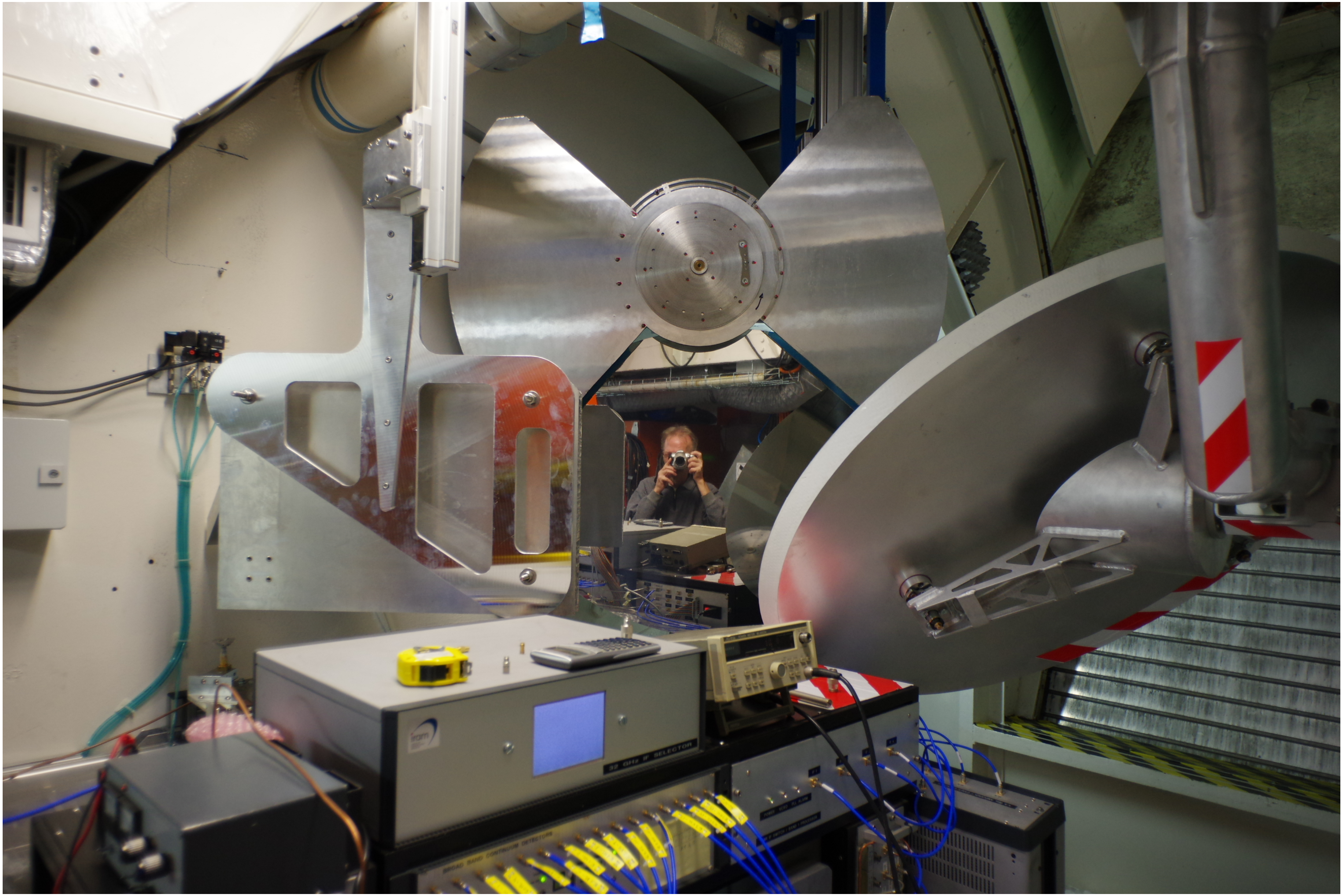

Single dish calibration: Contents & Literature

Contents:

1. Telescope: IRAM 30m telescope and others
2. Atmosphere
3. Point spread function of the telescope: the beam or antenna diagram
4. Heterodyne Receivers: temperature, sideband gain ratio
5. Antenna temperatures and “Chopperwheel” calibration
6. Telescope efficiencies: aperture, main beam, forward
7. Stability and observing switching modes

Literature:

- Lectures by ClemensThum, Pierre Hily-Blant, Bertrand Lefloch, Michael Bremer at previous IRAM summerschools in Spain and France
- **Tom Wilson and Susanne Huettemeister: Tools of Radio Astronomy**
- Jaap Baars 2007: The paraboloidal reflector antenna in radio astronomy
- Albert Greve & Michael Bremer 2010: Thermal design and thermal behaviour of radio telescopes and their enclosures

The atmosphere at the site of the 30m telescope

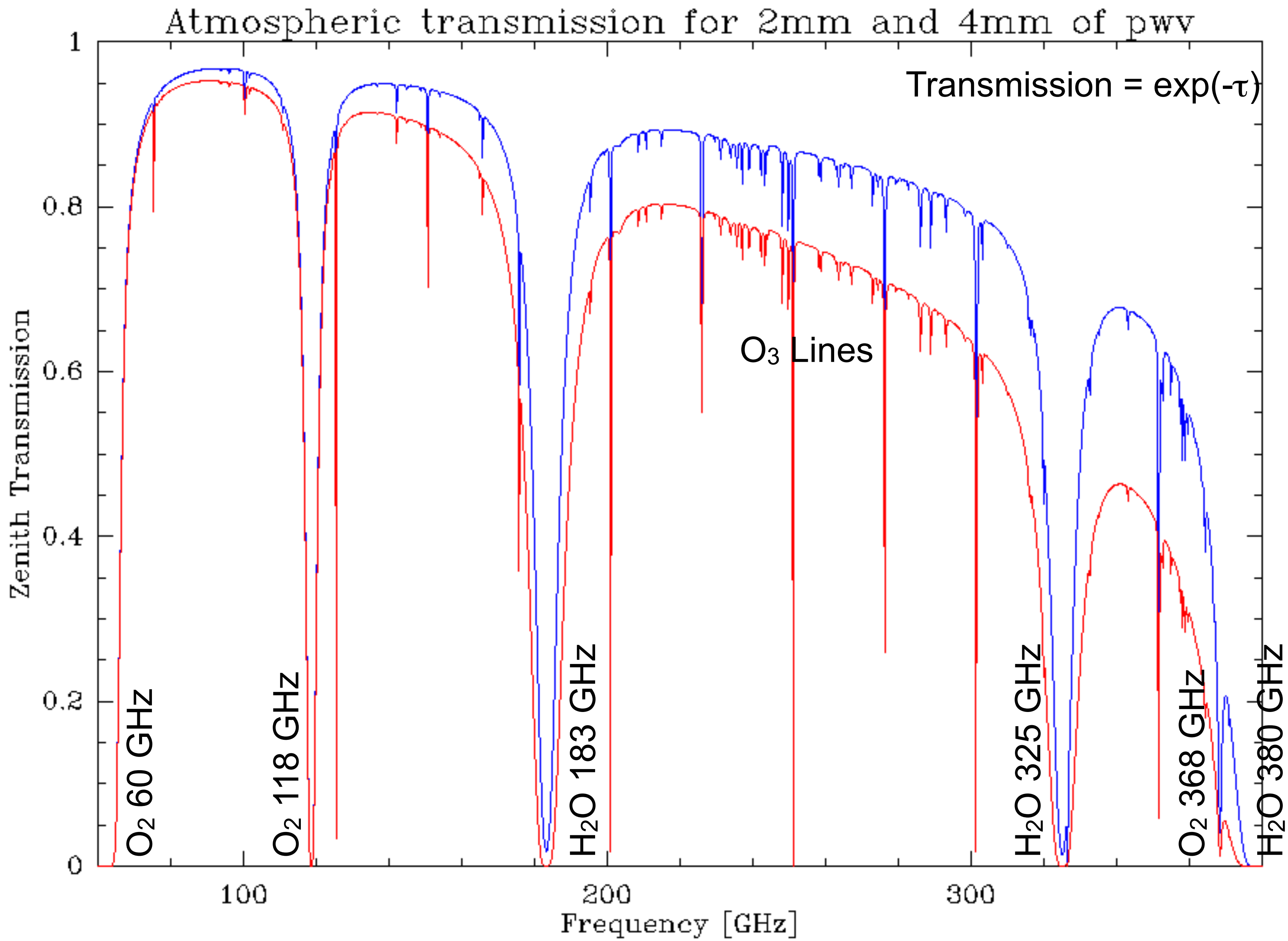

2850m altitude, Absorption by atmospheric H_2O, O_2, N_2, O_3, N_2O, NO_2, CO, …

Variable amount of precipitable water vapor (pwv), ATM model by J.Pardo & J.Cernicharo

The atmosphere at the site of the 30m telescope

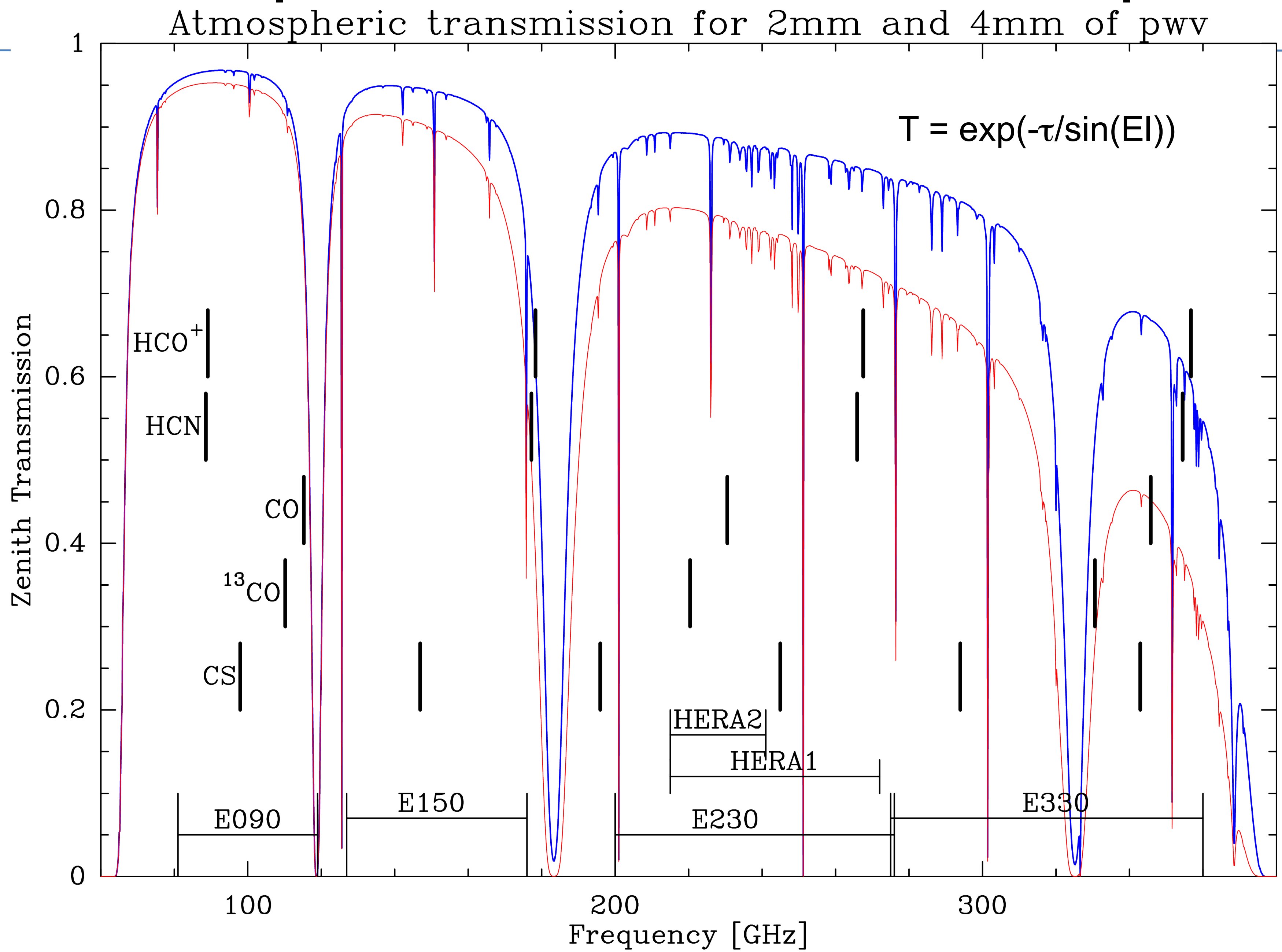

Atmospheric “windows” near 3, 2, 1, 0.8mm allow observations of the rotational lines of key interstellar species: e.g. HCO^+, HCN, CO, ^{13}CO, CS.

Taumeter water vapour statistics 2012 - 2017

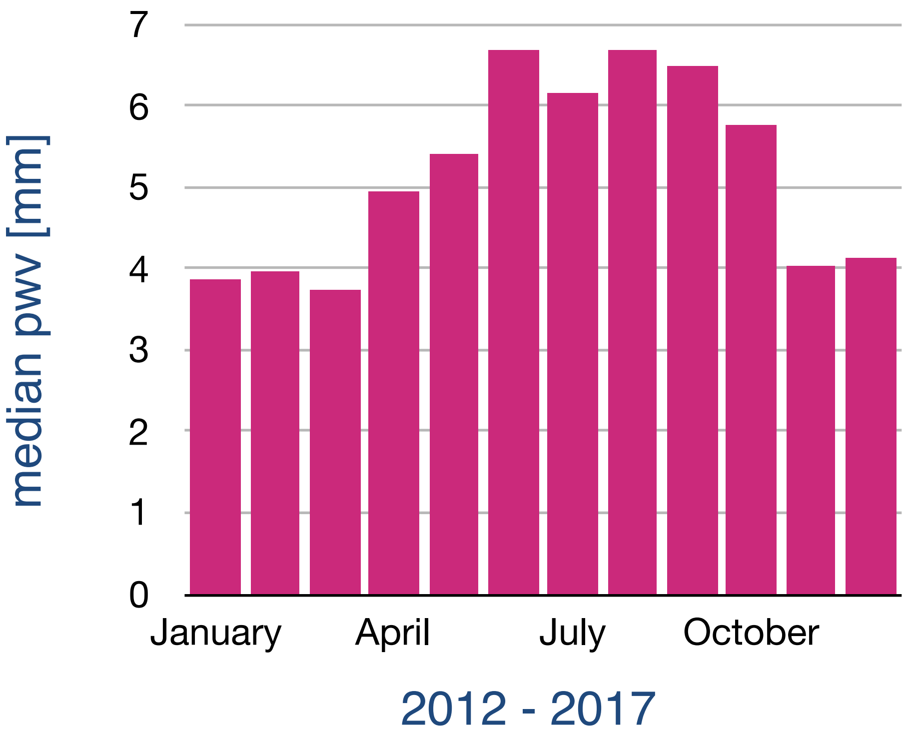

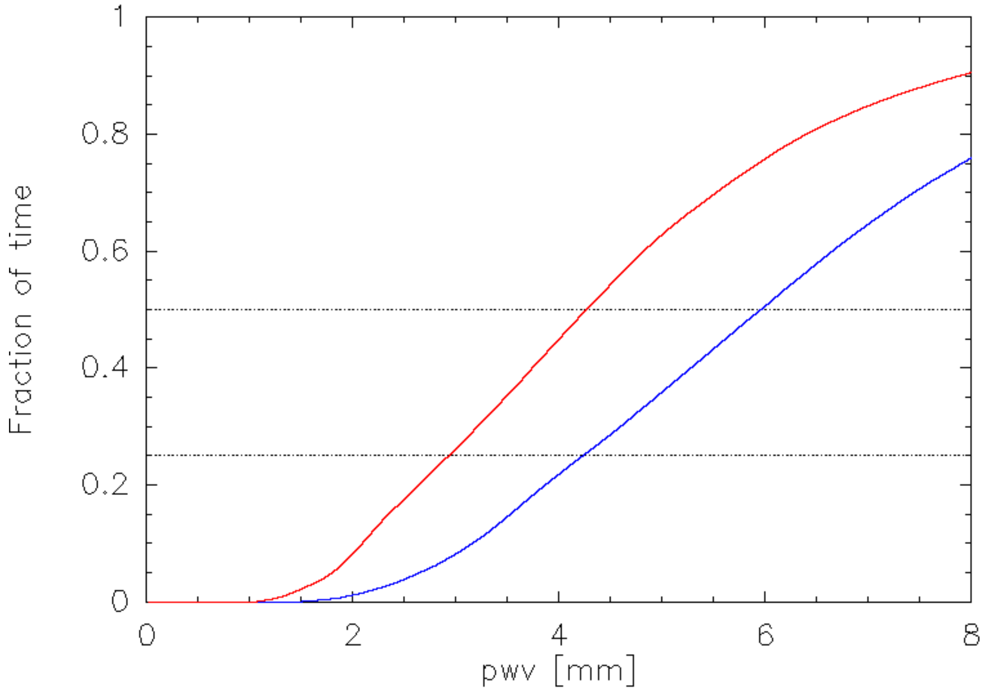

+ Summer: ⟨pwv⟩ ~ 6.5 mm
+ Winter: ⟨pwv⟩ ~ 4 mm

+ Summer months April - September: 50% < 6mm, 25% < 4.2mm
+ Winter months October - March: 50% < 4.2mm, 25% < 3mm

Single dish calibration: Contents & Literature

Contents:

1. Telescope: IRAM 30m telescope and others
2. Atmosphere
3. Point spread function of the telescope: the beam or antenna diagram
4. Heterodyne Receivers: temperature, sideband gain ratio
5. Antenna temperatures and “Chopperwheel” calibration
6. Telescope efficiencies: aperture, main beam, forward
7. Stability and observing switching modes

Literature:

- Lectures by ClemensThum, Pierre Hily-Blant, Bertrand Lefloch, Michael Bremer at previous IRAM summerschools in Spain and France
- **Tom Wilson and Susanne Huettemeister: Tools of Radio Astronomy**
- Jaap Baars 2007: The paraboloidal reflector antenna in radio astronomy
- Albert Greve & Michael Bremer 2010: Thermal design and thermal behaviour of radio telescopes and their enclosures

Intensity calibration: Antenna temperature I

Idea of the chopper wheel calibration (Penzias & Burrus 1973):

The calibration signal is the difference between an absorber at ambient temperature and the sky.

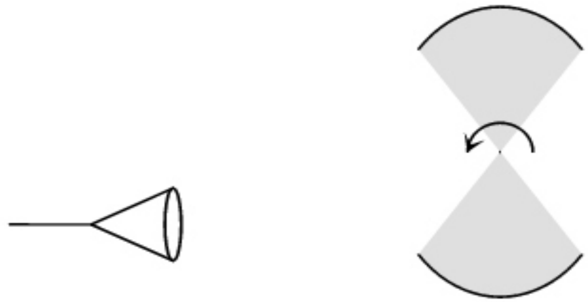

$V_{amb} = G\,(T_{amb} + T_{rec})$
$V_{sky} = G\,(T_{sky} + T_{rec})$
$V_{ON} = V_{sky} + G\,T_A$
$V_{OFF} = V_{sky}$

G is the varying factor to be calibrated out
Here, we neglect contribution from the ground (F_{eff}=1).

$$\Delta V_{cal} = V_{amb} - V_{sky} = G\,(T_{amb} - T_{sky}) = G\,(T_{amb} - T_{amb}\,(1 - e^{-\tau A})) = G\,T_{amb}\,e^{-\tau A}$$
$$\Delta V_{sig} = V_{ON} - V_{OFF} = G\,T_A = G\,T_A'\,e^{-\tau A}$$

$$T_A' = \frac{\Delta V_{sig}}{\Delta V_{cal}}\,T_{amb}$$

τ *is the zenith opacity*
A *is the airmass 1/sin(El)*
T_A' is the antenna temperature (of the source), *corrected for atmospheric extinction*

The simple ratio of signal and calibration, multiplied by the ambient temperature, gives the source temperature outside of the atmosphere, in first approximation (F_{eff}=1, T_{atm}=T_{amb}, G_{im}=1) !!
See "Radio Astronomy Techniques", Downes 1988

Receiver temperature

Observe two absorbers at two known temperatures:
+ hot or chop load at ambient temperature, Tchop
+ cold load at temperature of liquid Nitrogen, Tcold

$$\langle C_{\rm chop}\rangle = \langle c_{\rm off}\rangle + (T_{\rm chop} + T_{\rm rec}) * g$$
$$\langle C_{\rm cold}\rangle = \langle c_{\rm off}\rangle + (T_{\rm cold} + T_{\rm rec}) * g,$$

$$T_{\rm rec} = \frac{T_{\rm cold}\langle C_{\rm chop}\rangle - T_{\rm chop}\langle C_{\rm cold}\rangle}{\langle C_{\rm cold}\rangle - \langle C_{\rm chop}\rangle} - \langle c_{\rm off}\rangle \frac{T_{\rm chop} - T_{\rm cold}}{\langle C_{\rm chop}\rangle - \langle C_{\rm cold}\rangle}$$
$$= \frac{T_{\rm chop} - Y T_{\rm cold}}{Y - 1} \quad \text{with} \quad Y = \frac{\langle C_{\rm chop}\rangle - \langle c_{\rm off}\rangle}{\langle C_{\rm cold}\rangle - \langle c_{\rm off}\rangle}.$$

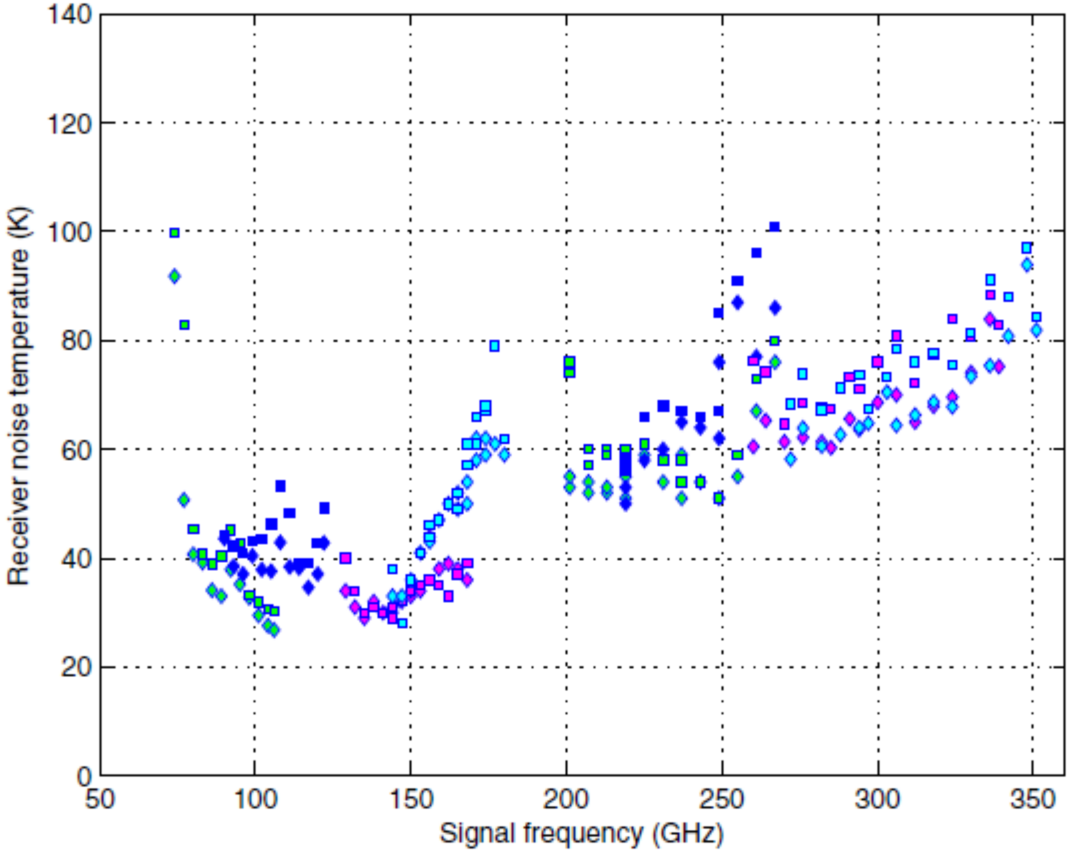

Parameters characterizing receivers:

+ receiver temperature T_{rec}
  (not a physical temperature!)
  Fundamental limit: $T_{rec} > h\nu/k$
  $h\nu/k$ = 11K at 230GHz
+ bandwidth
+ imageband rejection
+ stability

EMIR multiband mm-receiver
Carter, Lazareff et al. 2012

Hot/Cold/Sky Calibration

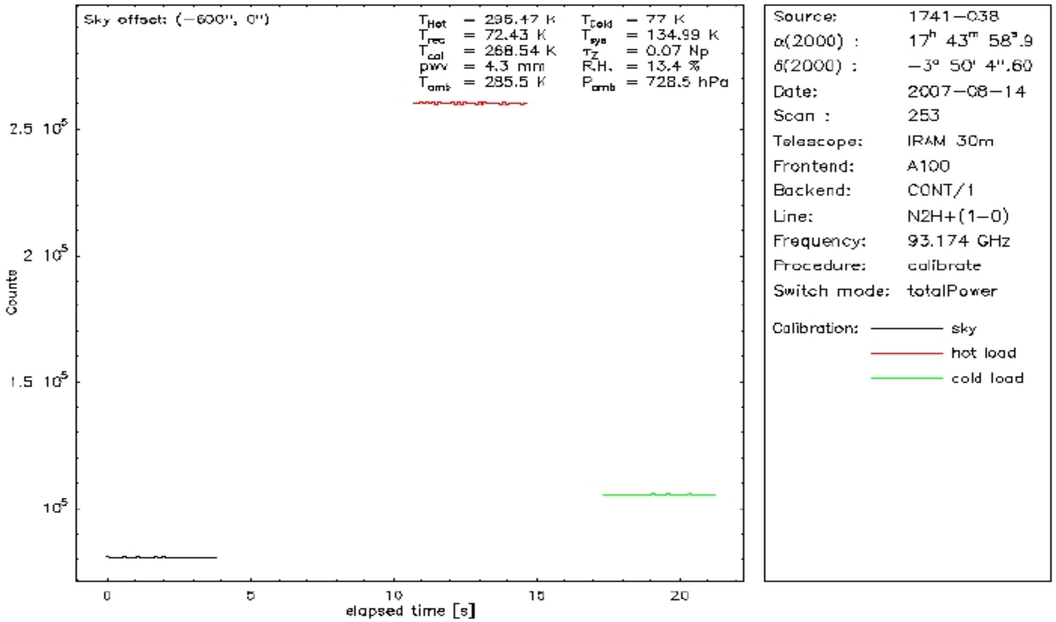

Continuum backend

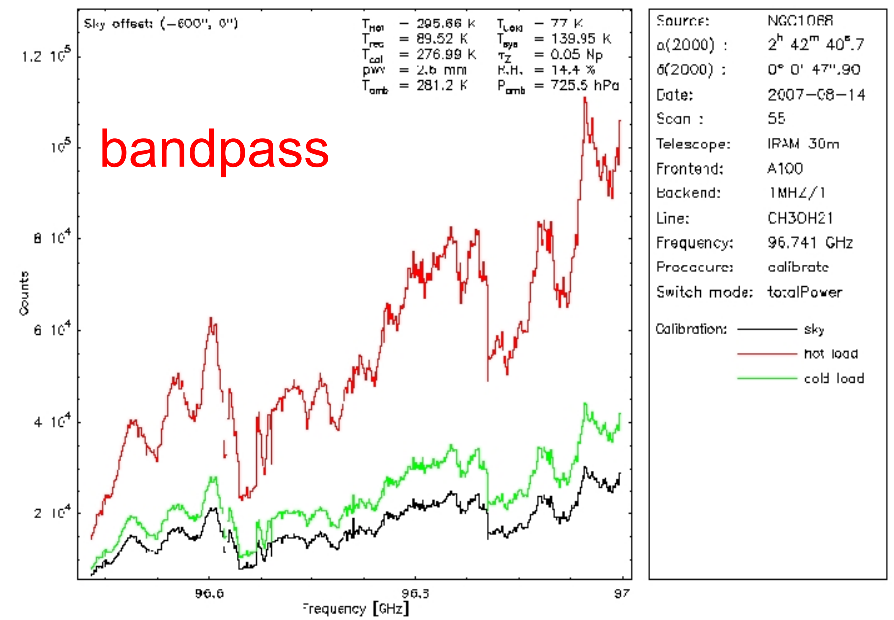

Spectrometer backend

input:

T_{HOT} sensor

T_{COLD} lookup table

T_{AMB} meteo station

G_{im} -13dB

Pressure meteo station

Humidity meteo station

output:

$T_{RX}(\nu)$, T_{CAL}, T_{SYS}, pwv, zenith opacity

(The atmospheric model ATM is used to correct for any opacity difference between signal and image band !)

Heterodyne receivers: Image band rejection

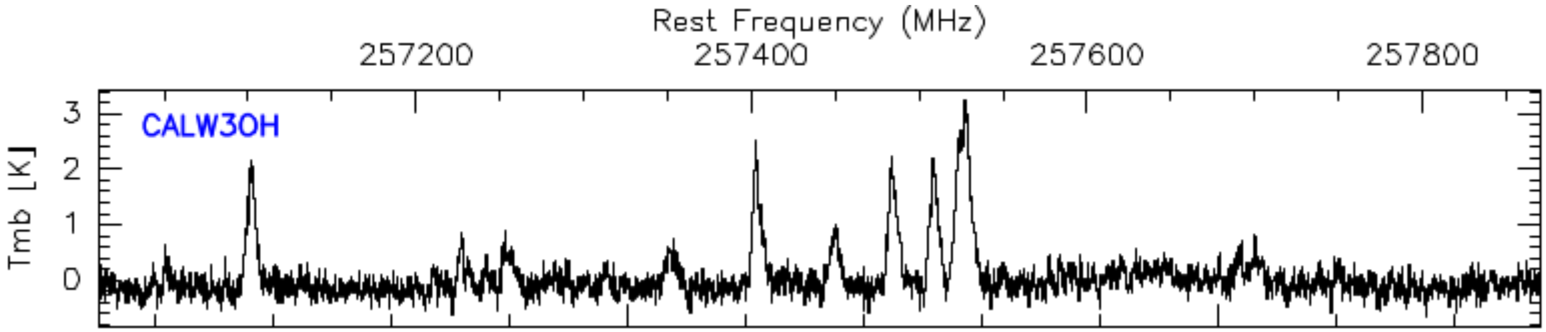

Frequency survey of the Galactic star forming region W3OH by Nicolas Biver using the dual-sideband mixers of the EMIR receiver band E230.

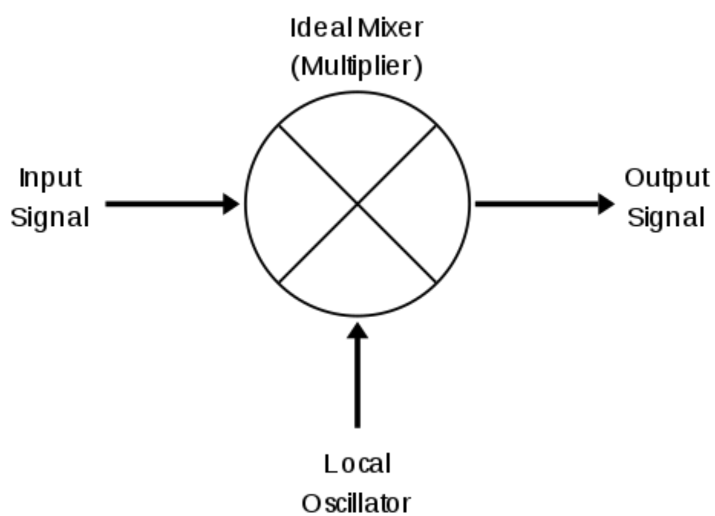

Heterodyne principle: single processing by mixing two frequencies to obtain the mixing product, the intermediate frequency $f_{IF}=f_1-f_2$.

Heterodyne receivers: Image band rejection

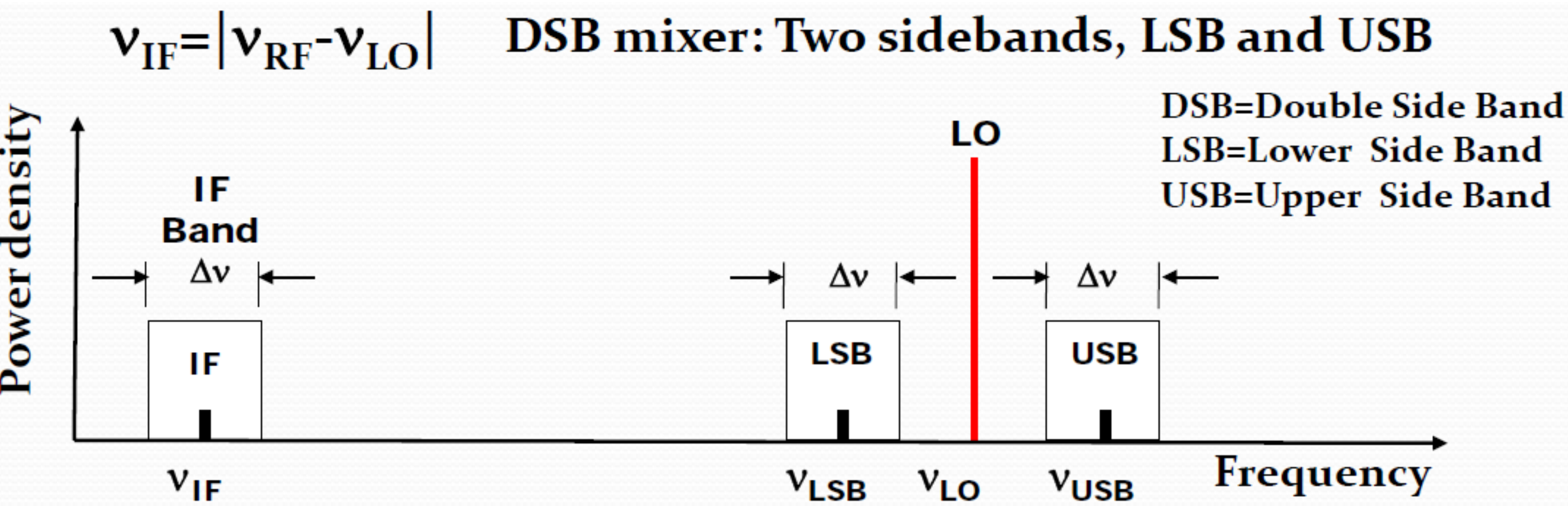

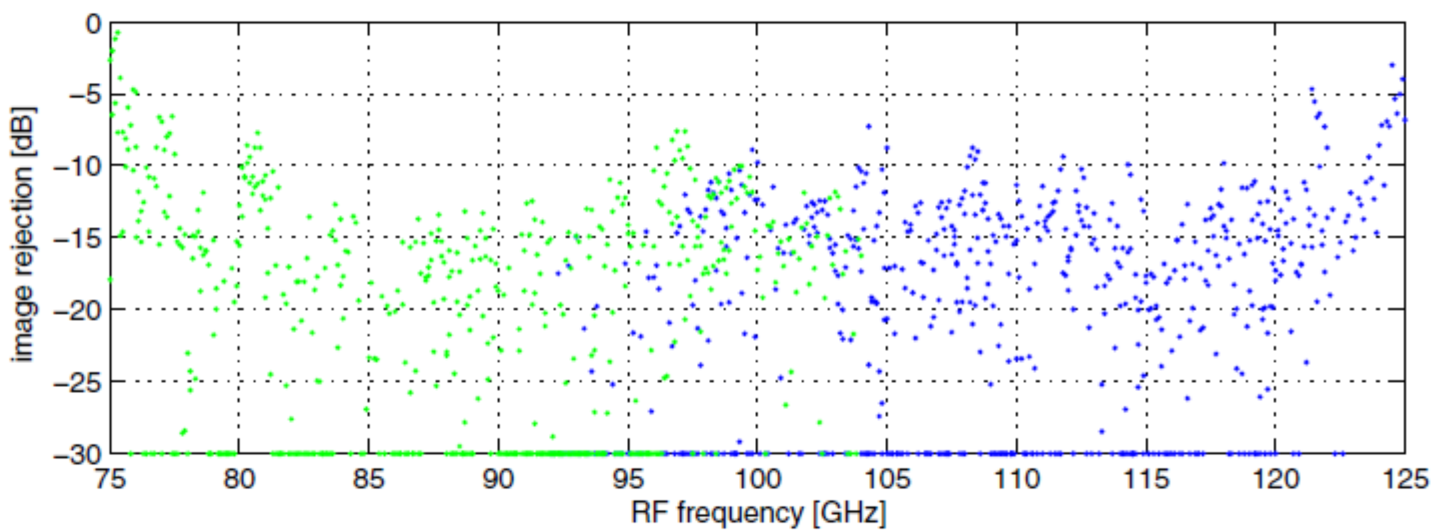

Detection of both sidebands.
Image band rejection:
$dB = -10 \log(I/I_0)$
Green: lower sideband operation
Blue: upper sideband operation

3mm band of EMIR, Carter, Lazareff et al. 2012

Temperatures in radio-astronomy

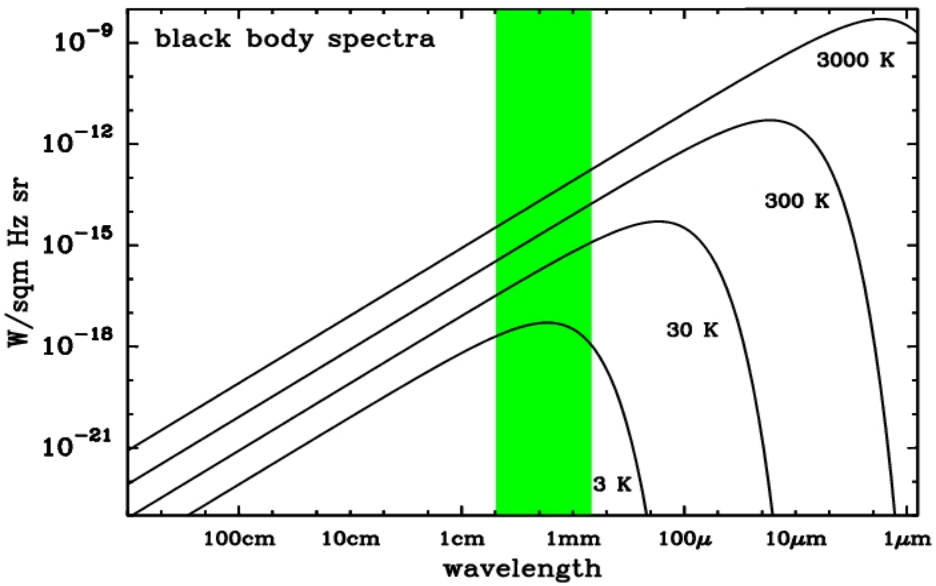

Black body radiation:

$$B_\nu(T) = \frac{2h\nu^3}{c^2} \frac{1}{e^{h\nu/kT} - 1}$$

Rayleigh-Jeans limit:

$$h\nu \ll kT \qquad B_{RJ}(\nu, T) = \frac{2\nu^2}{c^2} kT$$

$$\frac{\nu}{\mathrm{GHz}} \ll 20.84 \left(\frac{T}{\mathrm{K}}\right)$$

At mm wavelengths with its rather high frequencies, RJ approximation is not valid anymore for typical low temperatures of molecular clouds: 230 ~ 20.84 x 10K = 208.4

<u>Radiation temperature:</u>

$$J(T) = \frac{c^2}{2k\nu^2} I = \frac{h\nu}{k} \frac{1}{e^{h\nu/kT} - 1}$$

In the RJ-Limit: *J(T)=T.*
First order correction is 5.5K at 230GHz:

$$J_\nu(T_B) = T_B - \frac{h\nu}{2k}$$

In radio astronomy, the brightness is measured by the <u>brightness temperature</u> Tb. This is the temperature which would result in the given brightness/intensity if inserted into the RJ-Law:

$$T_b = \frac{c^2}{2k} \frac{1}{\nu^2} I_\nu = \frac{\lambda^2}{2k} I_\nu \, .$$

If the emitting source is not a thermodynamic black body, T_b will depend on frequency.

T_b is also used when the RJ-approximation is not valid.

Antenna temperature II: Deriving the calibration factor

$$T^*_{A,i} = T_{cal} * \frac{C_{source,i} - C_{atm,i}}{C_{chop,i} - C_{atm,i}} = T_{cal} * \frac{\Delta C_{source,i}}{\Delta C_{cal,i}} = T_{cal} * \frac{\text{signal}_i}{\text{gain}_i}.$$

$$C_{chop} = g\Big[G_s J(\nu_s, T_{chop}) + G_i J(\nu_s, T_{chop}) + T_{rec}\Big]$$

$$C_{atm} = g\Big(G_s\big[F_{eff} J(\nu_s, T_{sky}) + (1 - F_{eff}) J(\nu_s, T_{cab})\big] + G_i\big[F_{eff} J(\nu_i, T_{sky}) + (1 - F_{eff}) J(\nu_i, T_{cab})\big] + T_{rec}\Big).$$

$$J(\nu, T_{sky}) = J(\nu, T_{ATM})(1 - \exp(-\tau A)) + J(\nu, T_{bg}) \exp(-\tau A).$$

The source signal enters only through the signal sideband, but the atmosphere etc. enter through both sidebands.

$$\Delta C_{cal} = C_{chop} - C_{atm},$$

$$T^*_A = T_A \exp(\tau_s A) * \frac{1}{G_s F_{eff}} = T'_A \frac{1}{F_{eff}} \qquad \frac{T_{chop} - T_A^{sky}}{\langle C_{chop}\rangle - \langle C_{atm}\rangle} = \frac{T_{chop} - T_{cold}^{corr}}{\langle C_{chop}\rangle - \langle C_{cold}\rangle}.$$

$$\Delta C_{source} = C_{source} - C_{atm} = g T_A = g G_s F_{eff} \exp(-\tau_s A) T^*_A.$$

The calibration factor T_{cal} is now defined such that

$$T_{cal} = \frac{\Delta C_{cal}}{\Delta C_{source}} * T^*_A = \frac{\Delta C_{cal}}{g G_s F_{eff} \exp(-\tau_s A)}$$

and we finally find:

$$\begin{aligned} T_{cal} = \; & (1 + G_{im})\Big[J(\nu_s, T_{ATM}) - J(\nu_s, T_{bg})\Big] \\ & +(1 + G_{im})\Big[J(\nu_s, T_{cab}) - J(\nu_s, T_{ATM})\Big] \exp(\tau_s A) \\ & +G_{im}\Big[J(\nu_s, T_{ATM}) - J(\nu_s, T_{bg})\Big]\Big[\exp((\tau_s - \tau_i)A) - 1\Big] \\ & +(1 + G_{im})/F_{eff}\Big[J(\nu_s, T_{chop}) - J(\nu_s, T_{cab})\Big] \exp(\tau_s A) \end{aligned}$$

For: $J(T) = T \; (h\nu \ll kT) \quad T_{bg} = 0.$ ←

follows:

calibration factor:

$$T_{cal} = \frac{(1 + G_{im})}{F_{eff} * \exp(-\tau_s A)} * (T_{chop} - T_A^{sky})$$

Antenna temperature II

basic equation:

$$T_A^* = \frac{\Delta V_{sig}}{\Delta V_{cal}} T_{cal}$$

calibration factor:

$$T_{\rm cal} = \frac{(1+G_{\rm im})}{F_{\rm eff} * \exp(-\tau_{\rm s} A)} * (T_{\rm chop} - T_{\rm A}^{\rm sky})$$

For a derivation, see last slide. Antenna temperatures T_A^* are corrected for the atmosphere and for the forward efficiency F_{eff} . These are usually output by the calibration pipeline at the 30m.

Main beam temperatures:

$$T_{\rm mb} = \frac{F_{\rm eff}}{B_{\rm eff}} T_{\rm A}^*$$

Main beam temperatures are brightness temperatures of a source which fills the main beam.
The shape of the beam is explained in the next slides.

Single dish calibration: Contents & Literature

Contents:

1. Telescope: IRAM 30m telescope and others
2. Atmosphere
3. Point spread function of the telescope: the beam or antenna diagram
4. Heterodyne Receivers: temperature, sideband gain ratio
5. Antenna temperatures and “Chopperwheel” calibration
6. Telescope efficiencies: aperture, main beam, forward
7. Stability and observing switching modes

Literature:

- Lectures by ClemensThum, Pierre Hily-Blant, Bertrand Lefloch, Michael Bremer at previous IRAM summerschools in Spain and France
- **Tom Wilson and Susanne Huettemeister: Tools of Radio Astronomy**
- Jaap Baars 2007: The paraboloidal reflector antenna in radio astronomy
- Albert Greve & Michael Bremer 2010: Thermal design and thermal behaviour of radio telescopes and their enclosures

Telescope beam & point source sensitivity

Let a plane wave with power density S be intercepted by the telescope. A certain amount P_e is extracted from this wave by the antenna. Their ratio has the dimension of an area and is called effective aperture of the antenna:

$$A_e = P_e \, / \, |\langle \boldsymbol{S} \rangle|$$

$$A_e = \eta_A A_g$$

A_g = 707 m^2 for the 30m.

Total flux density of a source, S_ν measured in Jy: 1Jy = 10^{-26} W m^{-2} Hz^{-1}:

$$S_\nu = \int_{\Omega_s} I_\nu(\theta, \varphi) \cos\theta \, d\Omega, \qquad S_\nu = \frac{2 k \nu^2}{c^2} T_b \, \Delta\Omega$$

Mars scans in Azimuth & Elevation

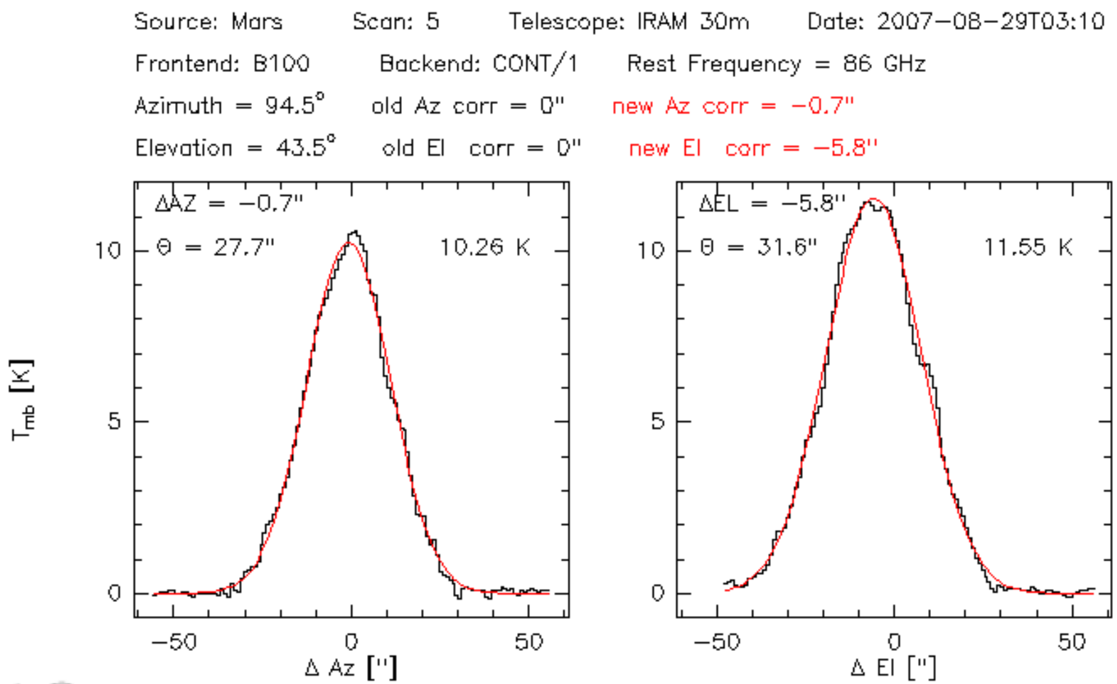

Power detected [W Hz^{-1}]:

$$w_\nu = k\, T_A' = \tfrac{1}{2}\, S_\nu A_{eff} = \tfrac{1}{2}\, \boldsymbol{\eta}_A A_g S_\nu$$

(factor ½ as only one polarisation is detected)

$$\eta_A = \frac{2k}{A_{geom}} \frac{T_A'}{S_\nu}$$

Point source sensitivity or aperture efficiency

Observation of point sources of known flux density. Small primary calibrators of well known brightness temperature: Uranus & Mars

Telescope beam pattern

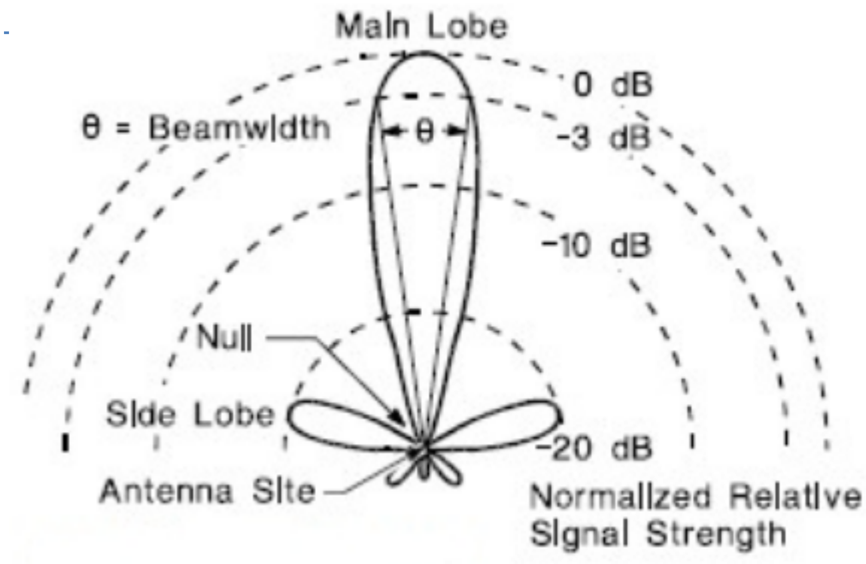

Diffraction at the 30m dish creates the beam pattern, i.e. the directional sensitivity or power pattern of the telescope. Its resolution is given by the half power beam width: HPBW = λ / D.

Normalized power pattern: $P_n(\vartheta,\varphi) = \frac{1}{P_{\max}} P(\vartheta,\varphi)$

Beam solid angle:

$$\Omega_A = \iint_{4\pi} P_n(\vartheta,\varphi)\, d\Omega$$

Main beam solid angle:

$$\Omega_{MB} = \iint_{\substack{\text{main}\\\text{lobe}}} P_n(\vartheta,\varphi)\, d\Omega$$

Main beam efficiency: $\eta_B = \frac{\Omega_{MB}}{\Omega_A}$

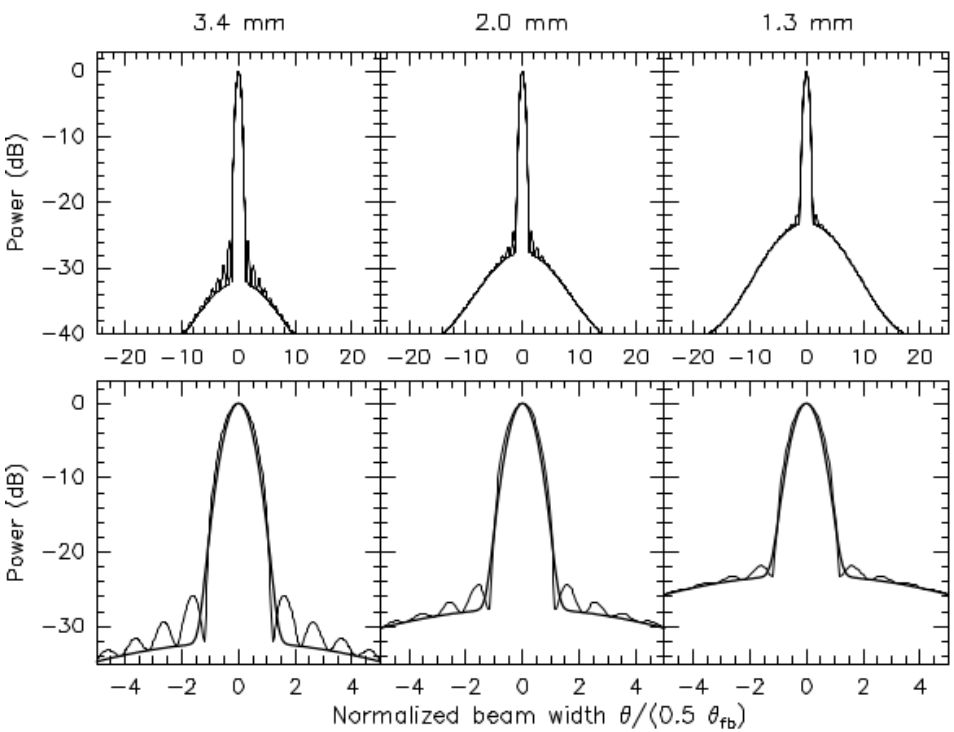

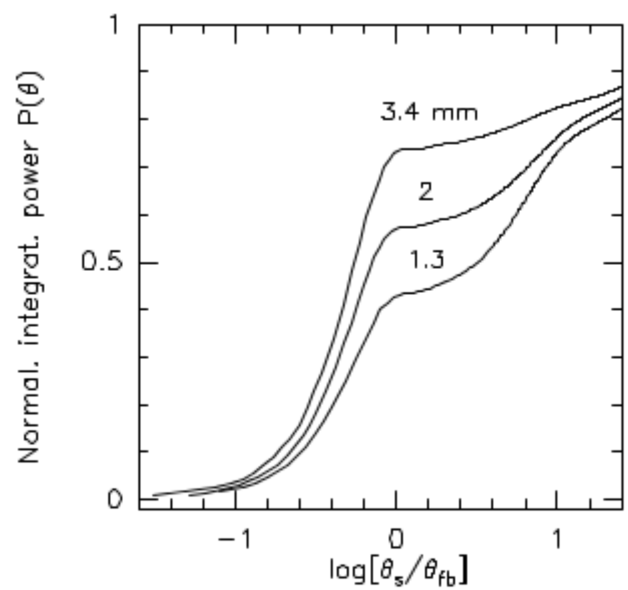

Beam of the 30m telescope (Greve, Kramer, Wild 1998)

Reciprocity theorem: The normalized power received and the normalized transmitted power patterns are identical.

Why modify the illumination with a taper ?

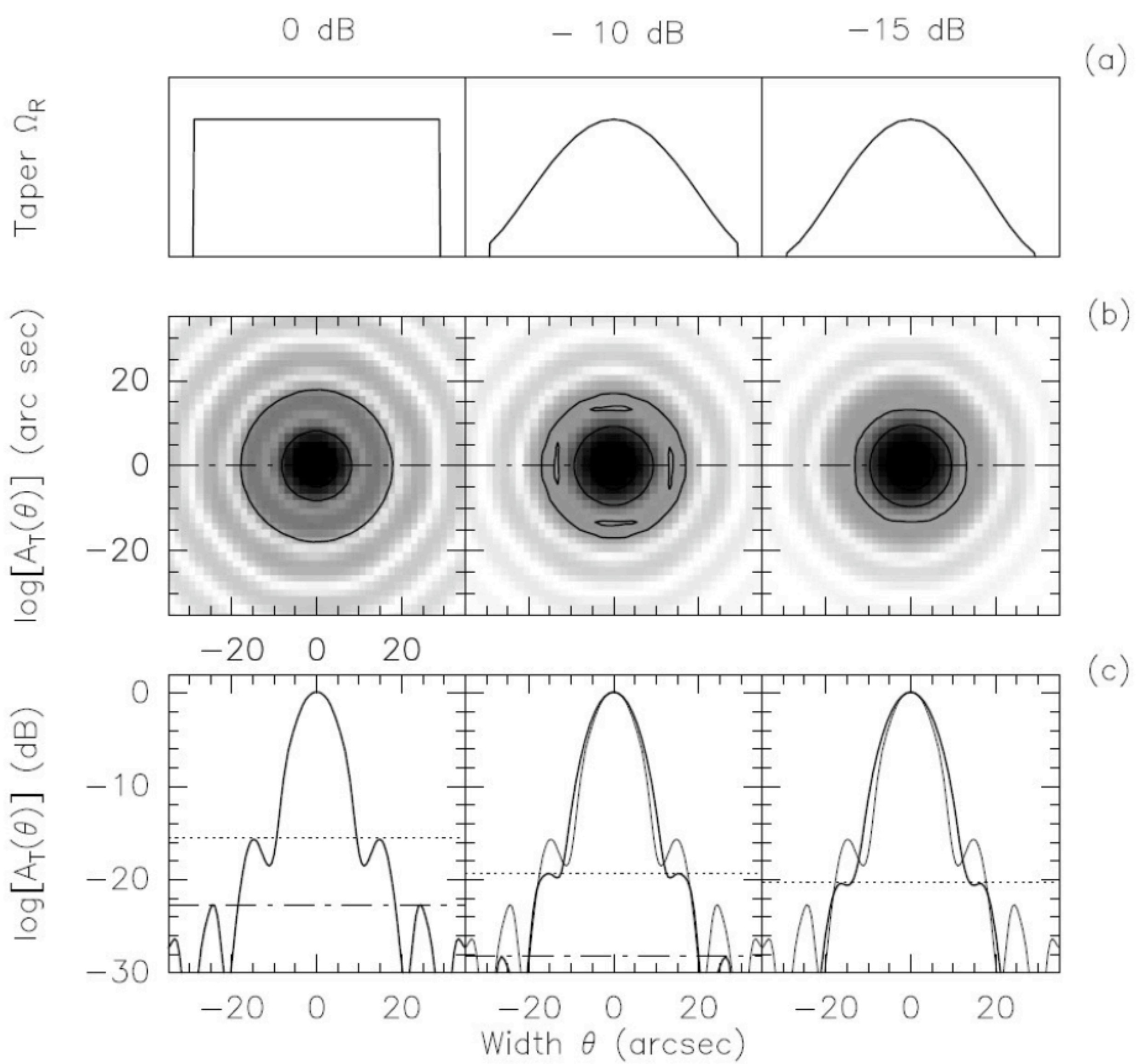

(a) Taper across the aperture of the main reflector Eq.(12.12), the value of the edge taper is indicated. (b) Focal plane beam pattern $A_T(\theta,\phi)$ (in log–scale). (c) Cut through the beam pattern $A_T(\theta,\phi)$. The dashed line shows the level of the 1st side lobe, the dashed–dotted line the level of the 2nd side lobe.

Taper function:
Gaussian or parabolic

Beam pattern = FFT(illumination)

Beam size (FWHM):
$\theta_{mb}=\alpha\, \lambda/D$ [rad]

with α = 1.0 … 1.3, depending on taper

Full width (diameter to 1st minimum):
$\theta_{fb} \approx 2.2\, \theta_{mb}$

A "typical" single dish antenna observes one point.

Measuring the extended beam pattern

Observations of the Moon edge allow to measure the beam pattern (Kramer, Penalver, Greve 2013):

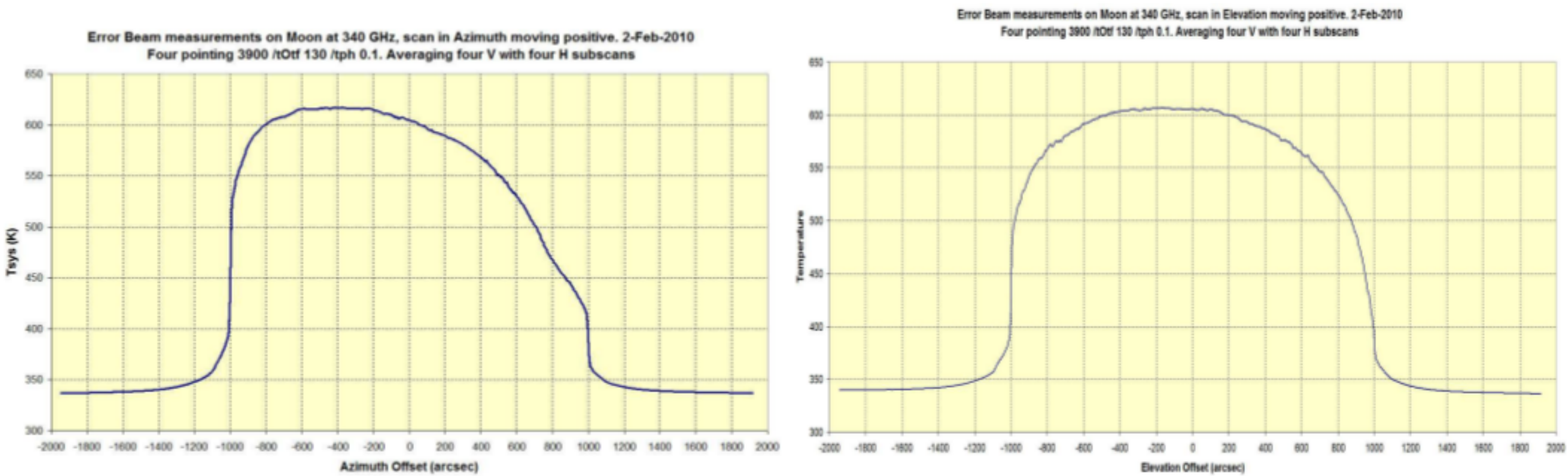

Figure 1: Scan of the Moon at 340 GHz in Azimuth (Left) and Elevation (Right).

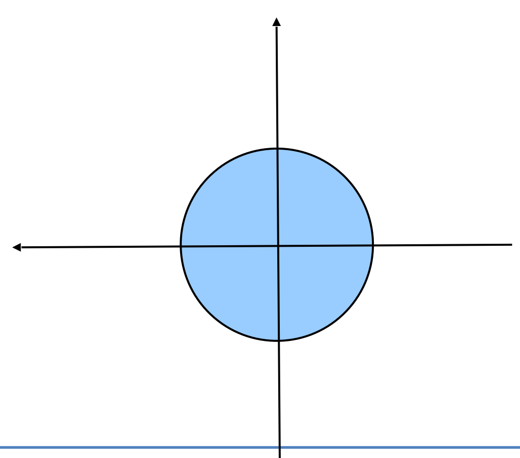

Repeated for different frequencies.

Close to ideal conditions:
+ Very low water vapour,
+ second half of the night,
+ ~50deg elevation.

Differentiation leads to the composite beam profile.

30m beam pattern

Observations of the Moon edge allow to measure the beam pattern (Kramer, Penalver, Greve 2013):

Red points show observed composite beam profile. Black curves show best fitting models. Blue curves show situation described in Greve et al. 1998.

Beam models include
+ main beam, plus
+ three Gaussian error beams, and a
+ model of panel buckling.

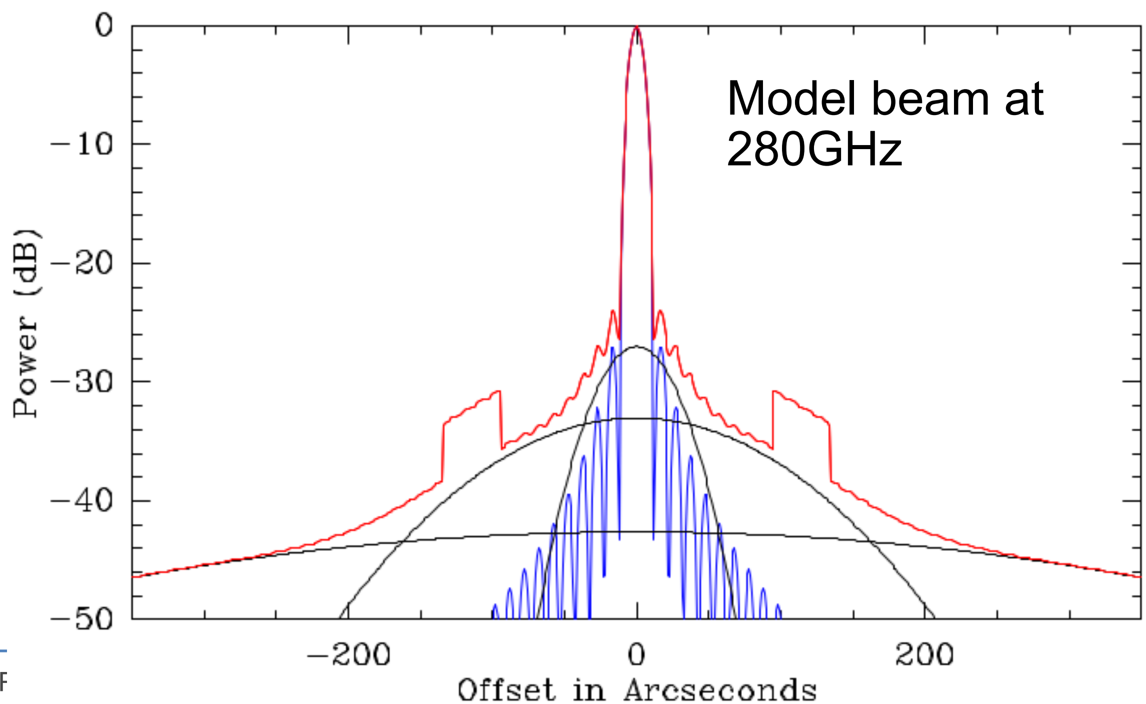

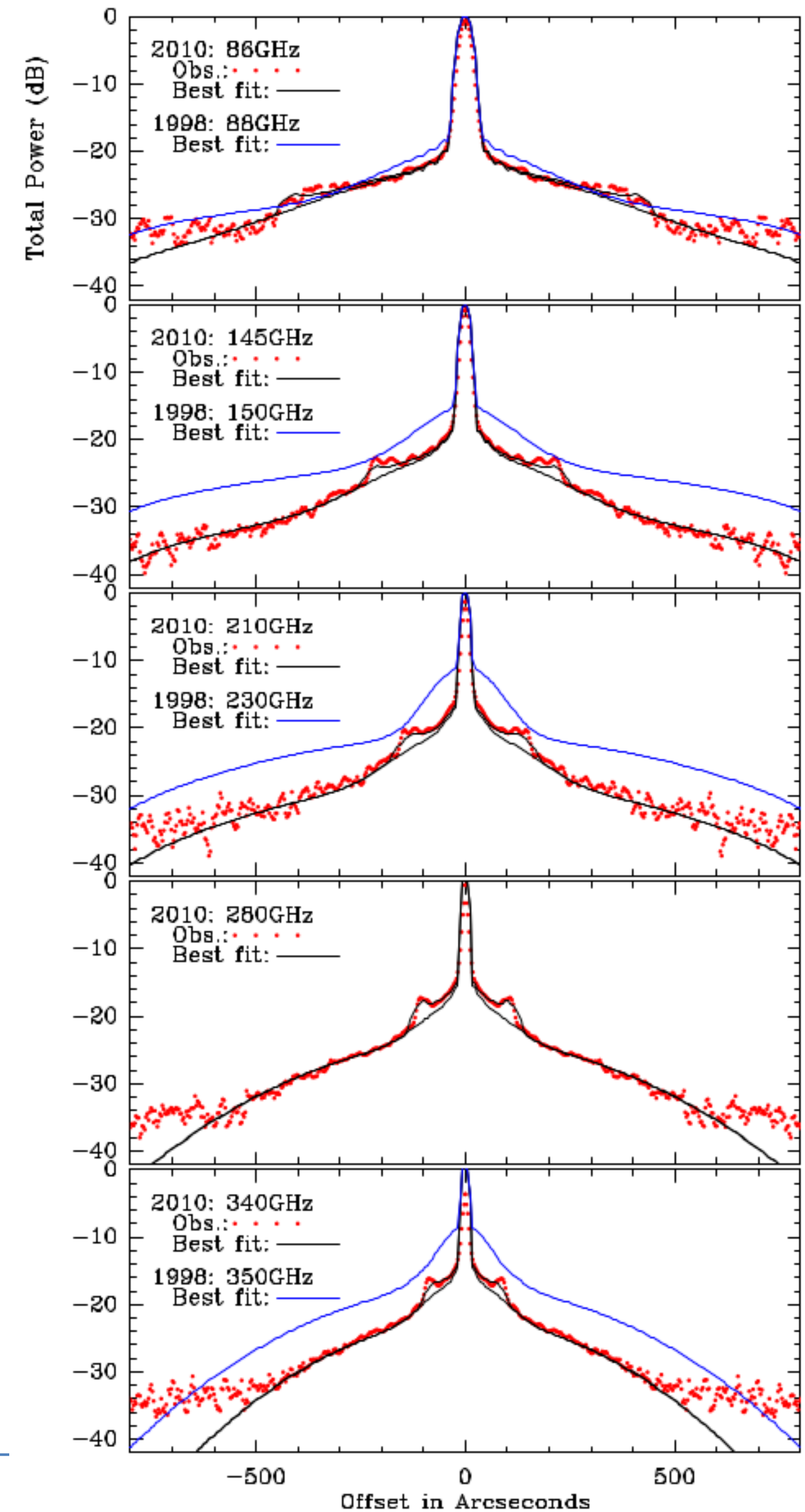

Telescope efficiencies

Telescope efficiencies:

+ Main beam efficiency $\eta_B = \frac{\Omega_{MB}}{\Omega_A}$

+ Forward efficiency: $\eta_l = \frac{\Omega_{2\pi}}{\Omega_A}$

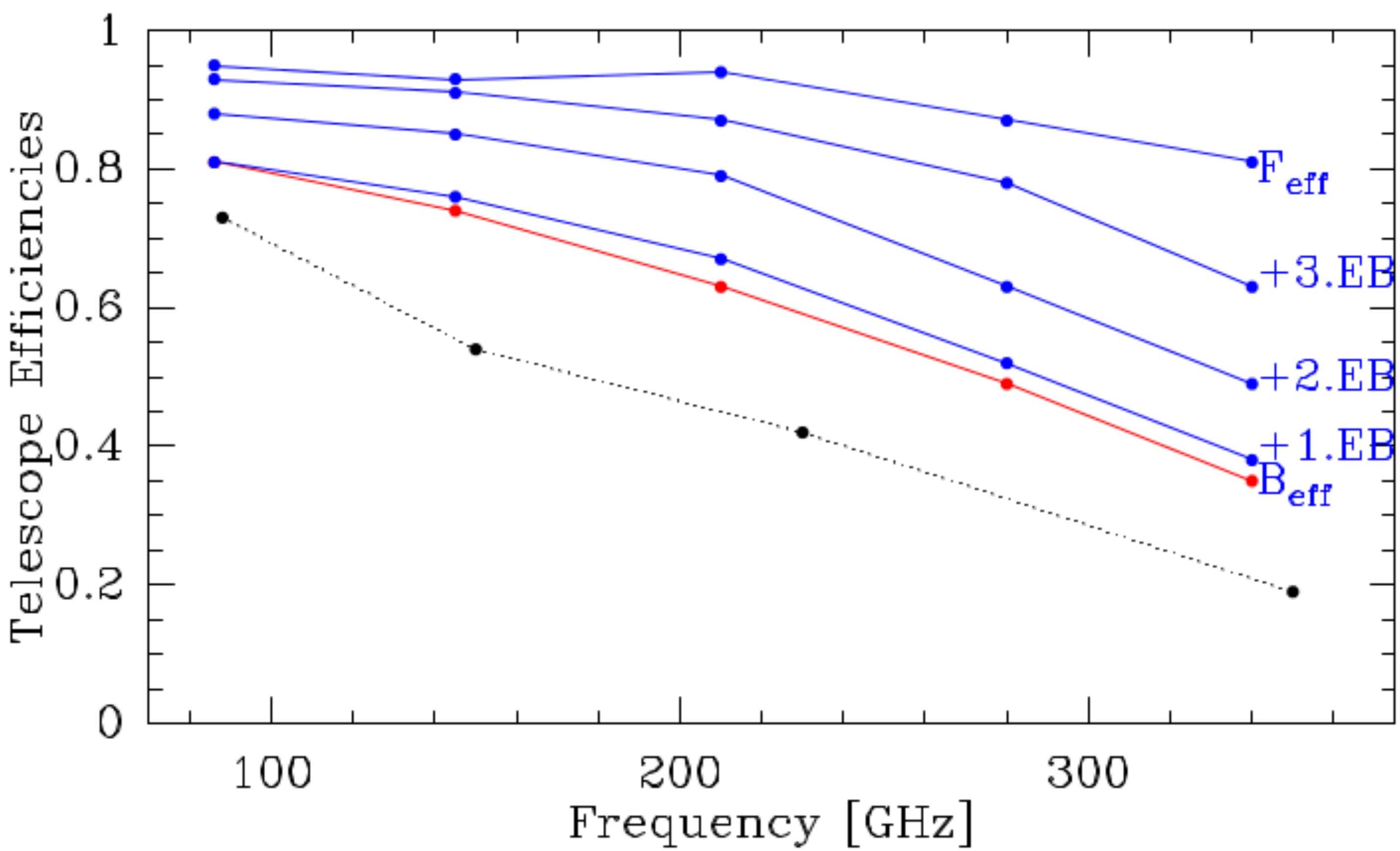

Widths of the main beam and the errorbeams

Half power beam width of the main beam and of the errorbeams:

$\Theta = \lambda / D$ or $\theta * \nu =$ const. (Constant illumination of the primary.)

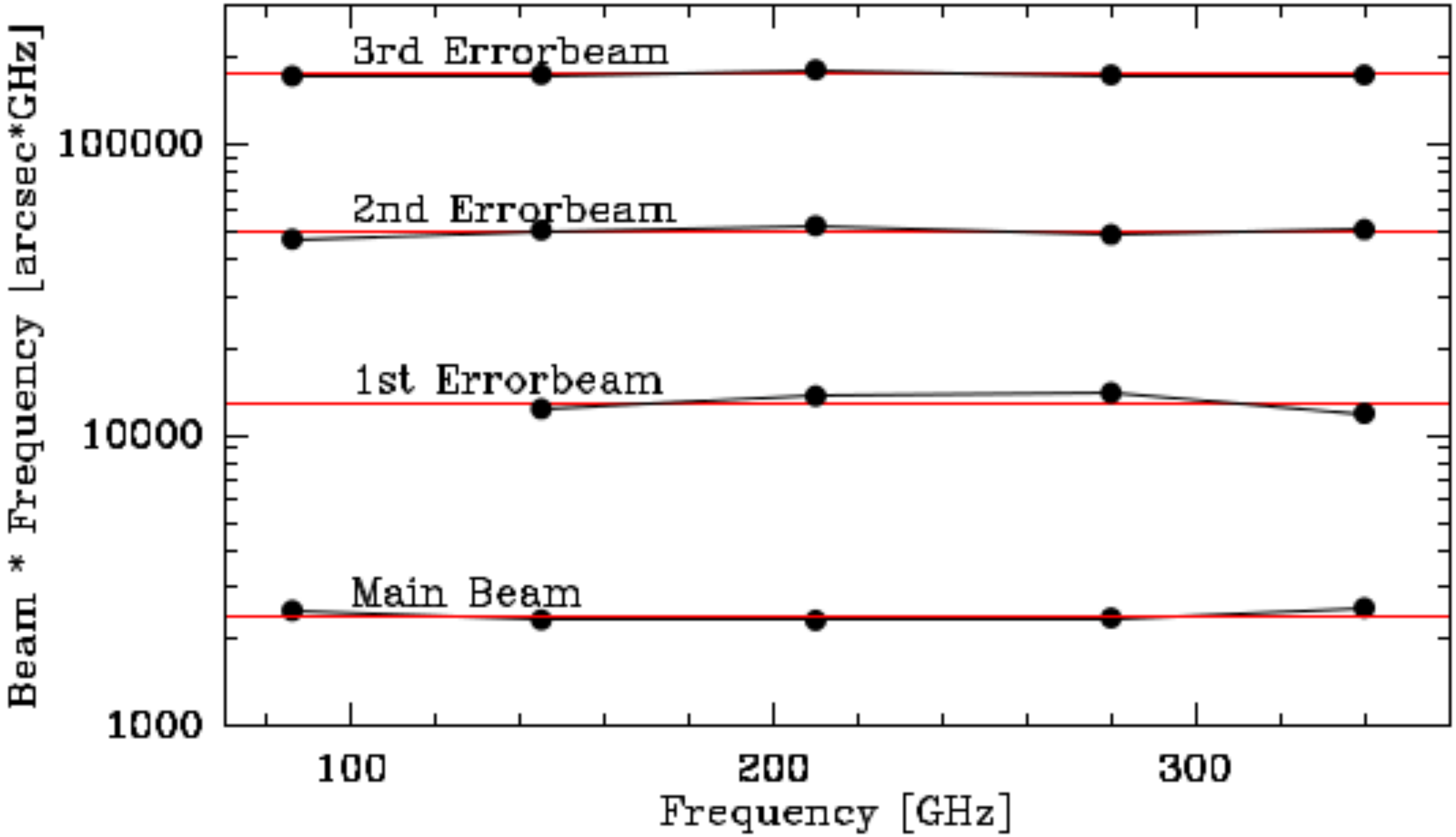

Main beam: HPBW/arcsec = 2460/Frequency/GHz:

21.4" at 115 GHz

10.7" at 230 GHz

7" at 345 GHz

2-dimensional beam pattern

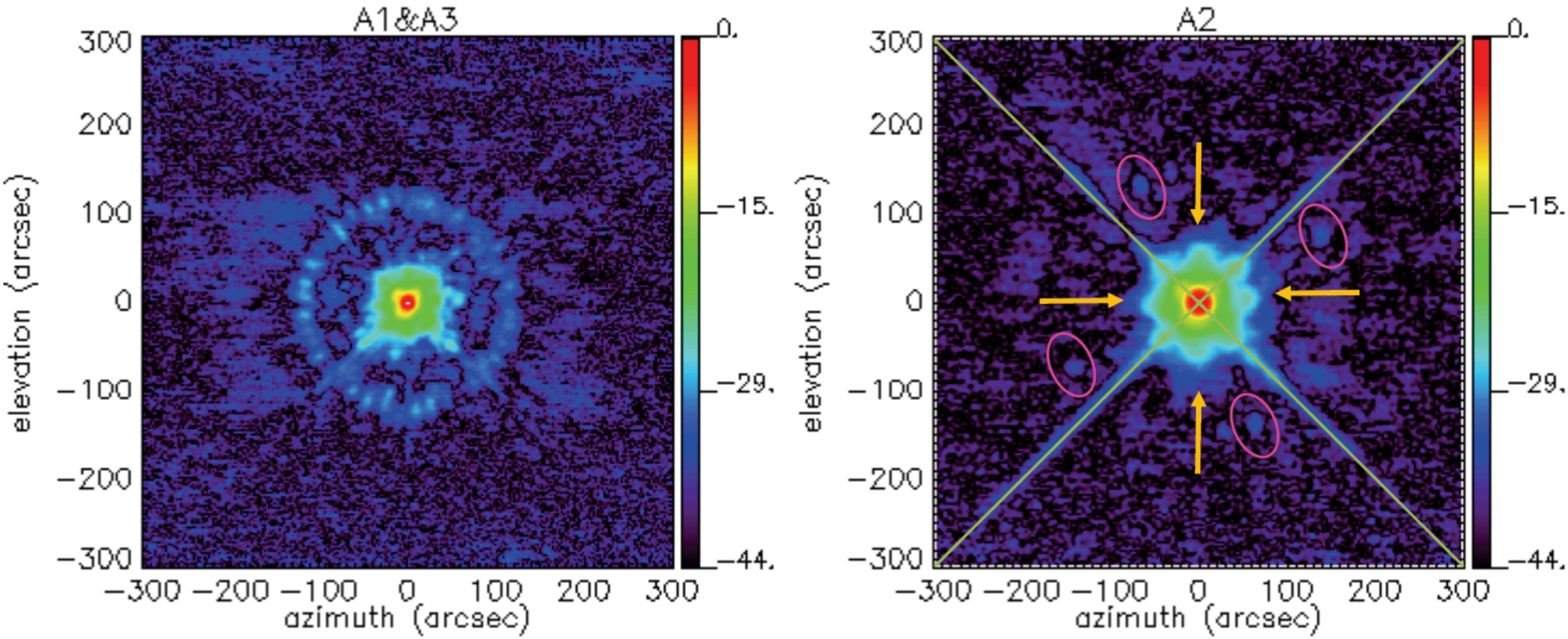

30m beam patterns over 10’x10’ at 1mm (left) and at 2mm (right) measured with NIKA2 (Adam et al. 2018). The colour scale is logarithmic and shows dB.

Single dish calibration: Contents & Literature

Contents:

1. Telescope: IRAM 30m telescope and others
2. Atmosphere
3. Point spread function of the telescope: the beam or antenna diagram
4. Heterodyne Receivers: temperature, sideband gain ratio
5. Antenna temperatures and “Chopperwheel” calibration
6. Telescope efficiencies: aperture, main beam, forward
7. Stability and observing switching modes

Literature:

- Lectures by ClemensThum, Pierre Hily-Blant, Bertrand Lefloch, Michael Bremer at previous IRAM summerschools in Spain and France
- **Tom Wilson and Susanne Huettemeister: Tools of Radio Astronomy**
- Jaap Baars 2007: The paraboloidal reflector antenna in radio astronomy
- Albert Greve & Michael Bremer 2010: Thermal design and thermal behaviour of radio telescopes and their enclosures

Observing modes: switching overcomes drifts

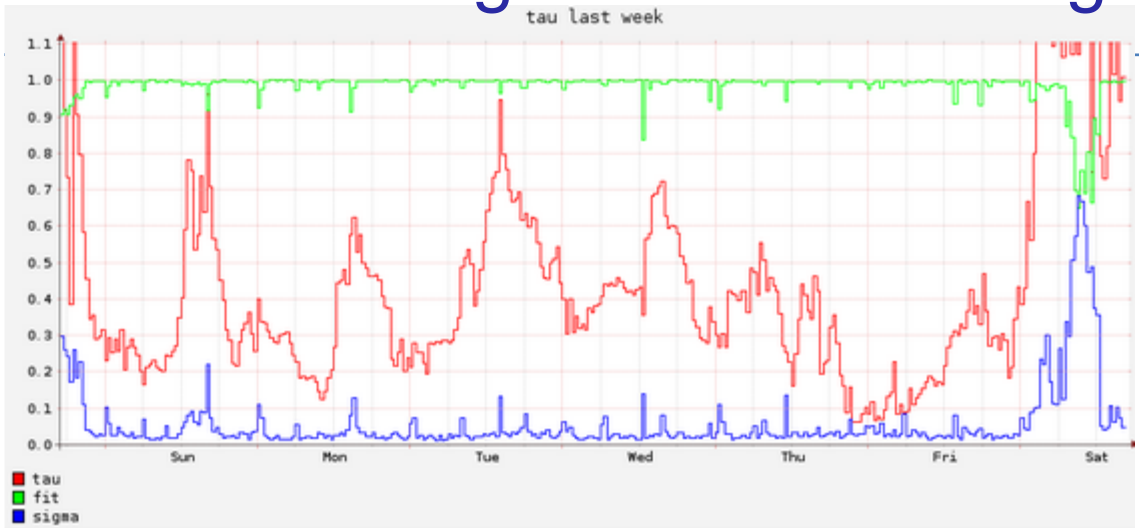

Example of measured zenith opacities at 225GHz by the IRAM taumeter on the Pico Veleta (red).

$T_{sys} = T_A + T_{sky} + T_{spillover} + T_{rx}$

$T_A \ll T_{sys}$ (most of the time)

T_A	$\leq$	1 K
T_{sky}	~	30 K (at 3mm)
$T_{spillover}$	~	20 K
T_{Rx}	~	50 K (at 3mm)

The enemies:
- sky emission fluctuations
- receiver gain fluctuations

Solutions for single pixel receivers:
switching between two positions on the sky or between two frequencies

- position switching (SWtotal, ONOFF, ~1 minute)
- wobbler switching (SWwobbler, ONOFF, ~1 second)
- frequency switching (SWfrequency, TRACK, ~200msec)

Depending on the stability times, fast switching is preferred.

Drifts and Allan variance

Frequency survey of W3OH by N.Biver

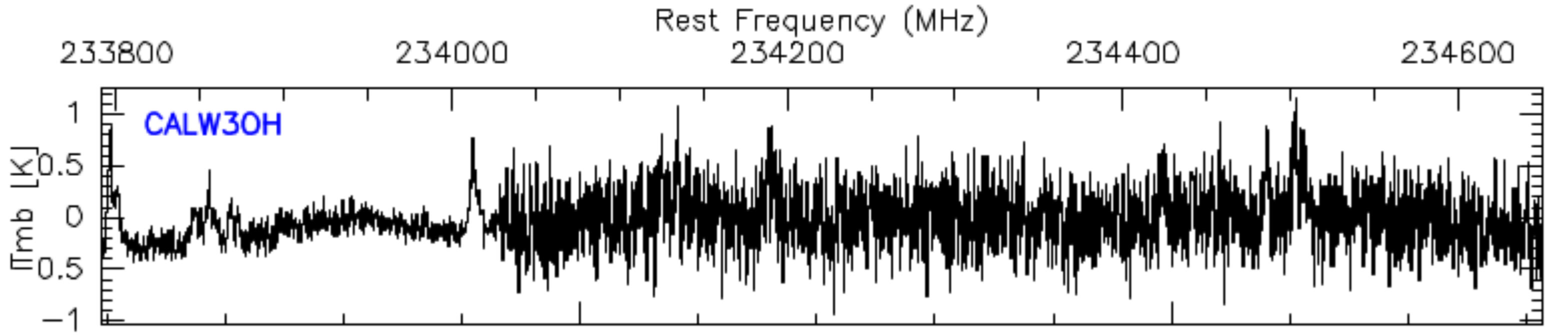

Drifts require switched observations, i.e. loop of reference and cali-bration observations to overcome drifts of atmosphere, receiver, IF-Chain, Backend.

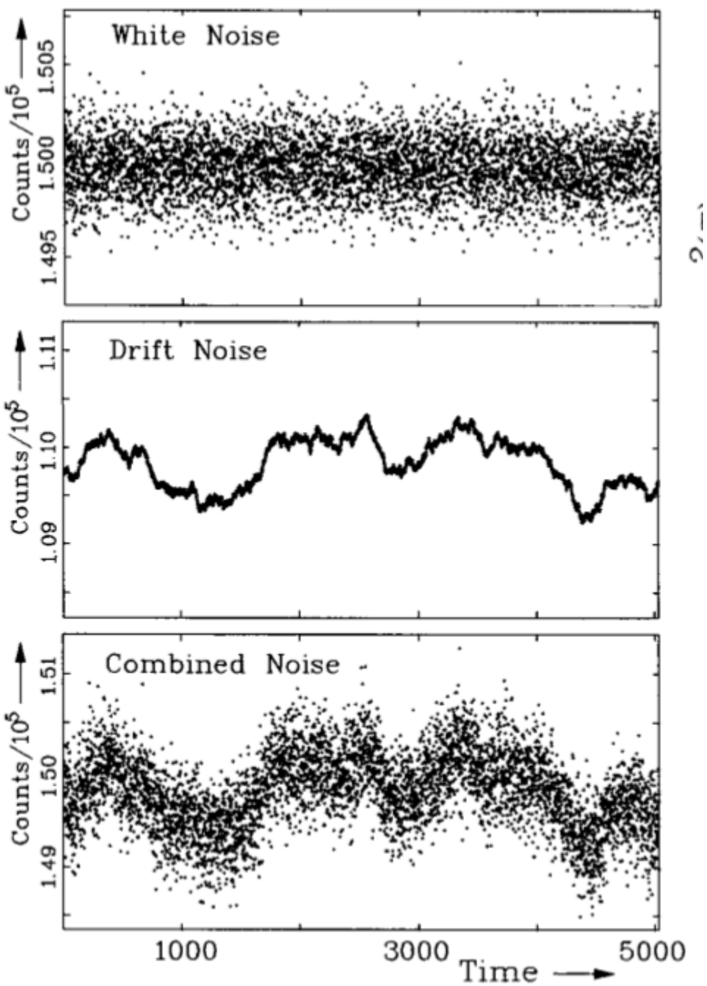

Artificial data (Schieder & Kramer 2001)

Allan variance quantifies the drift:

$$d = x_s - x_r \qquad \sigma_A^2(T) = 1/2\langle d^2 \rangle$$

Distinguish between spectroscopic and total power Allan variance

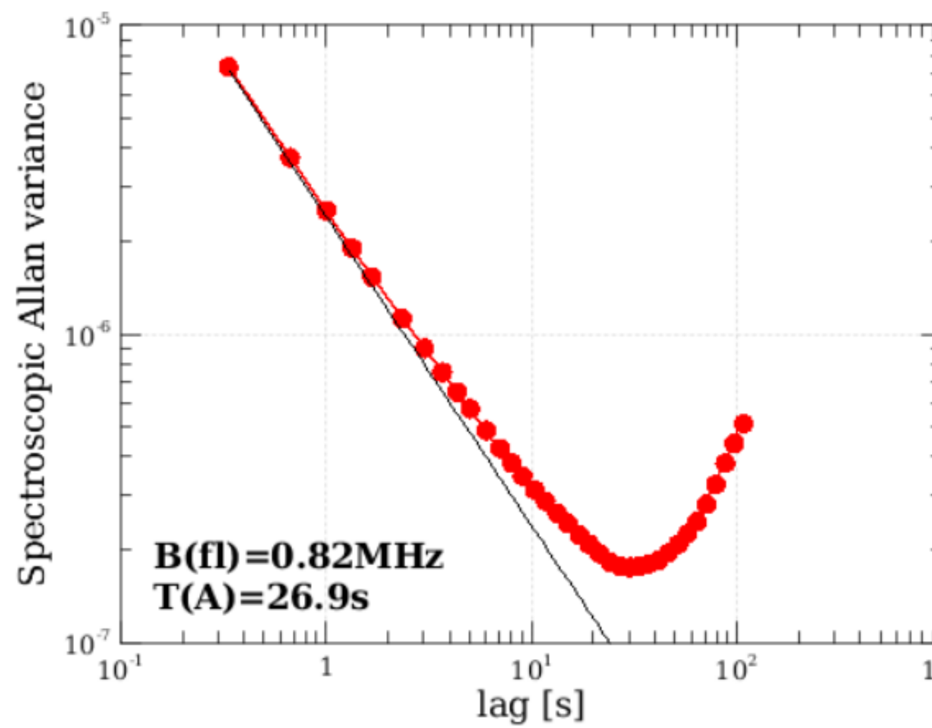

lag (or T) is the integration interval

Cycles

Drifts require loop of reference and calibration observations:

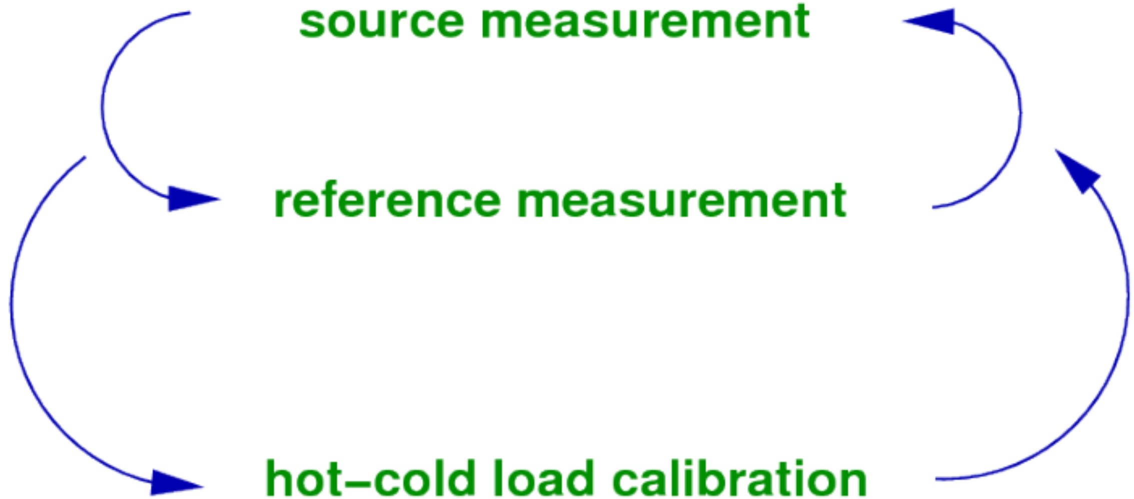

+ Schieder & Kramer, A&A, 2001, 373, 746
+ Ossenkopf, A&A, 2008, 479, 915
+ Ossenkopf, A&A, 2009, 495, 677

Determined in principle by Allan stability time t_A, which depends on the goal resolution of the observation:

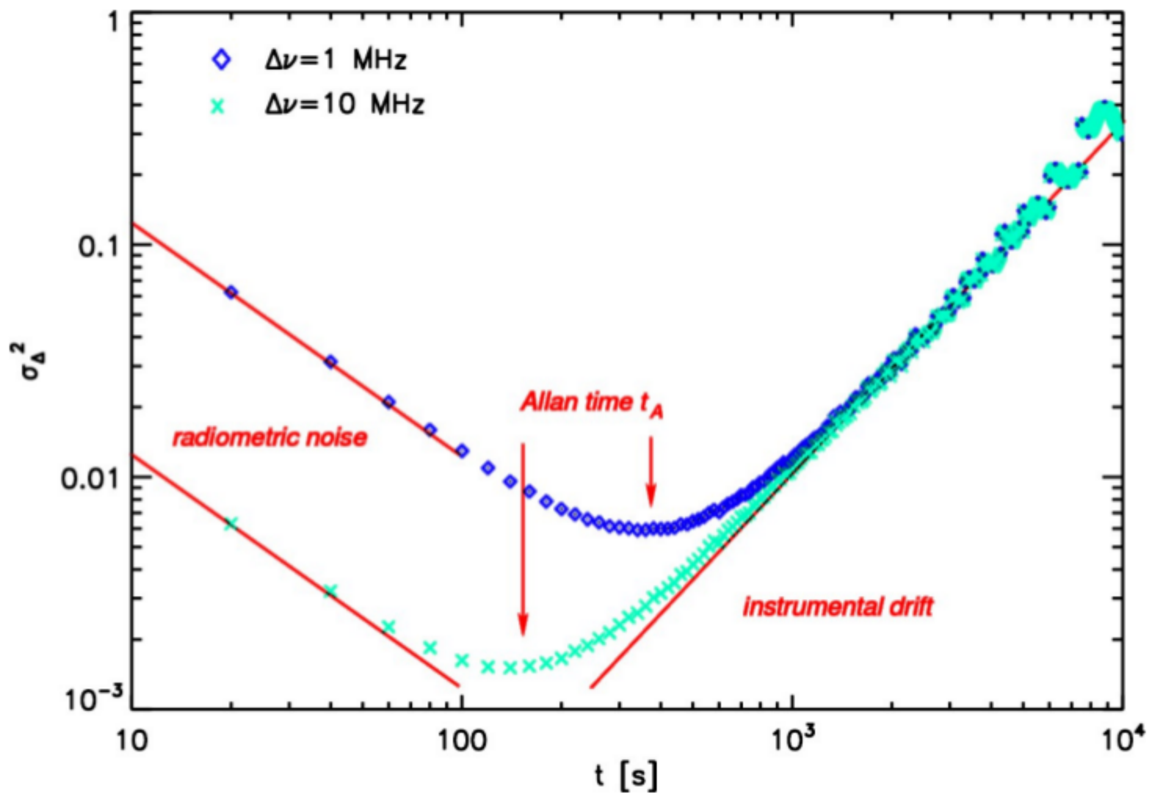

Typical cycle times at the 30m:

Source/reference with wobbler:
1-2 seconds

Source/reference with telescope:
1-2 minutes

Hot/cold/sky calibration:
10-15 minutes

Example: sequence of on-the-fly observations

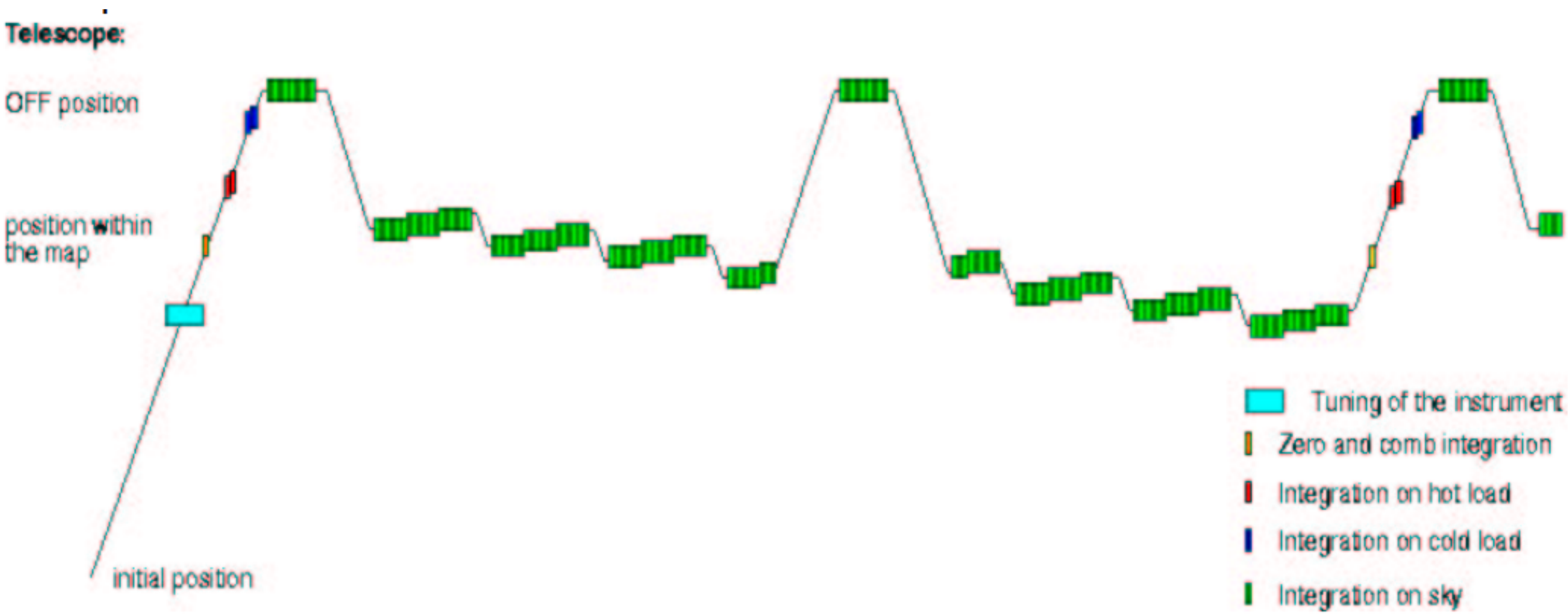

Ossenkopf, HIFI observing modes

Observing modes at the 30m

iram
Institut de Radioastronomie Millimétrique

	Single point observations (tracked)	Spectral scans	Mapping observations (on-the-fly)
Position switching	Pointed position switch onoff	Frequency overlap for image lines, Gim	Nyquist or lower sampling observations
Beam switching	Pointed DBS, compact source	Frequency overlap for image lines, Gim	---
Frequency switching	Optimize frequency throw to suppress standing waves	For scarcely sampled line sources	Not often used

Not implemented:
- + load chop,
- + sky reference for frequency switching,
- + balanced off-positions

Single dish calibration: Contents & Literature

Contents:

1. Telescope: IRAM 30m telescope and others
2. Atmosphere
3. Point spread function of the telescope: the beam or antenna diagram
4. Heterodyne Receivers: temperature, sideband gain ratio
5. Antenna temperatures and "Chopperwheel" calibration
6. Telescope efficiencies: aperture, main beam, forward
7. Stability and observing switching modes

Literature:

- Lectures by ClemensThum, Pierre Hily-Blant, Bertrand Lefloch, Michael Bremer at previous IRAM summerschools in Spain and France
- **Tom Wilson and Susanne Huettemeister: Tools of Radio Astronomy**
- Jaap Baars 2007: The paraboloidal reflector antenna in radio astronomy
- Albert Greve & Michael Bremer 2010: Thermal design and thermal behaviour of radio telescopes and their enclosures

Aperture efficiency - sensitivity of the antenna

(cf. Baars, 2007)

Product of all losses: $\eta_A = \eta_i \eta_s \eta_r \eta_e \eta_f \eta_b \eta_{ge}$

With the efficiency components:

+ η_i = **illumination efficiency** of the aperture by the feed function ("taper")
  Most important contributor to aperture efficiency.
+ η_s = **spillover efficiency** of the feed
  Power detected from beyond the edge of subreflector and primary.
  Partly cold sky, partly warm background, elevation dependent.
+ η_r = **radiation efficiency** of the reflector surface (ohmic losses)
  relevant for high frequency and for mirrors with paint layer
+ η_e = **surface error efficiency** ("Ruze loss", also called scattering efficiency)
  Small scale, randomly distributed deviations of the reflector from the perfect paraboloidal shape cause phase errors over the aperture. Leads to Ruze formula.
+ η_f = **focus error efficiency** (both lateral and axial defocus)
  Non-optimum foci cause large scale, systematic phase errors over the aperture.
  Observer tries to minimize these by regular focus observations and corrections.
+ η_b = **blocking efficiency** due to quadrupod, subreflector.
  Partial shadowing of the aperture by central subreflector and support structure:
  (a) plane-wave blocking, (b) spherical wave blocking.
+ η_{ge} = **gain-elevation efficiency** describing the change with elevation

Aperture efficiency - illumination

(Baars, 2007)

Product of all losses: $\eta_A = \eta_i \eta_s \eta_r \eta_e \eta_f \eta_b$

+ η_i **= illumination efficiency** of the aperture by the feed function ("taper")
  Most important contributor to aperture efficiency.

Ratio of the gain of the antenna to that of a uniformly illuminated aperture. For a Gaussian illumination and an edge taper of -12dB, $\eta_i = 0.87$ (Fig.4.4. in Baars 2007).

The edge taper <u>increases</u> the resolution or half power beamwidth (HPBW): θ_A **= b (λ / D)**
In good approximation:
$b = 1.269 - 0.566\,\tau + 0.534\,\tau^2 - 0.208\,\tau^3$
with the edge taper τ with T/dB = 20 log(τ) and $0<\tau<1$.
For T = -12dB, $\tau = 0.25$, b ~ 1.15, i.e. the beam is broadened by ~12%.

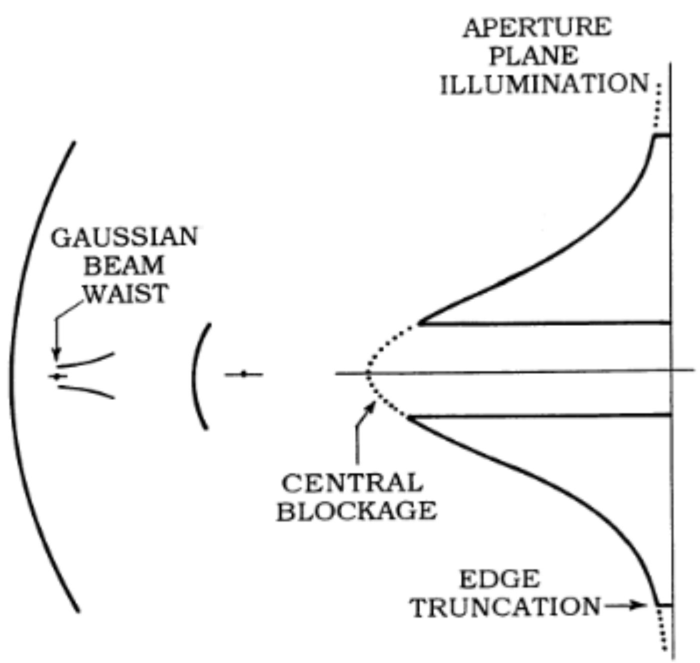

P.Goldsmith, 1999

On the other hand, the level of the sidelobes of the diffraction pattern is <u>reduced</u>. For example, the level of the 1st sidelobe is reduced from -17.5dB to -23dB for an edge taper of -12dB.

Aperture efficiency - spillover

Product of all losses: $\eta_A = \eta_i \eta_s \eta_r \eta_e \eta_f \eta_b$

+ η_s = **spillover efficiency** of the feed
  Power detected from beyond the edge of subreflector and primary.
  Partly cold sky, partly warm background, elevation dependent.

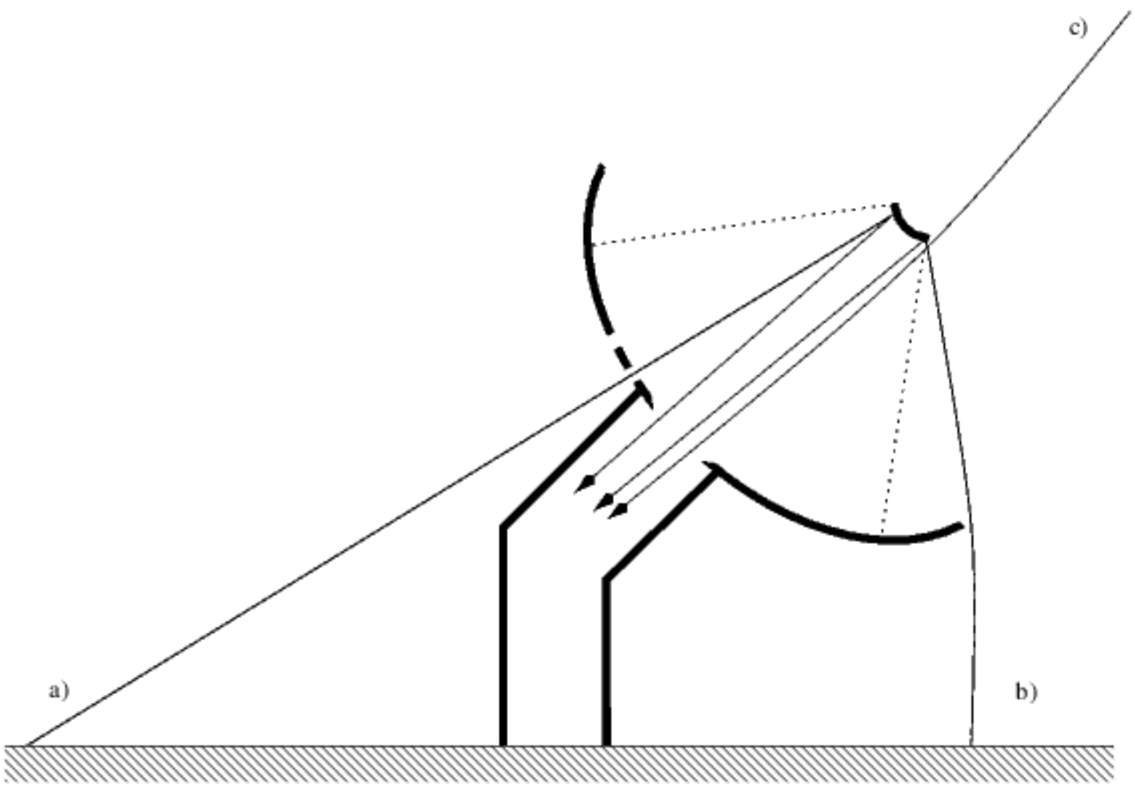

Hiyama 1998, Univ. zu Koln

Aperture efficiency - blocking

Product of all losses: $\eta_A = \eta_i \eta_s \eta_r \eta_e \eta_f \eta_b$

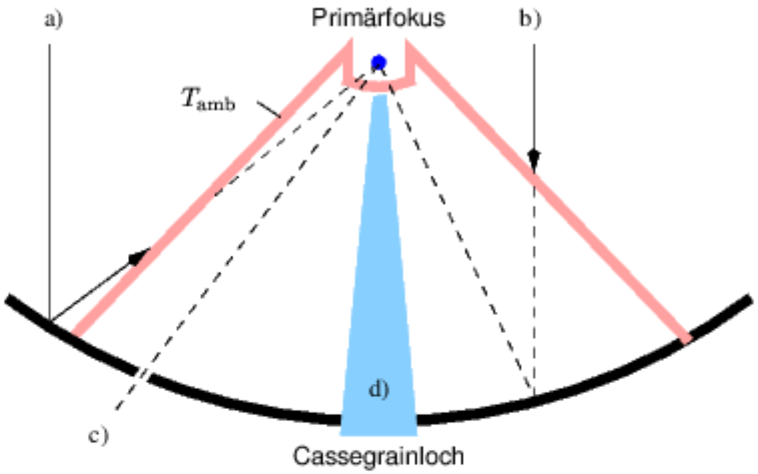

+ η_b = **blocking efficiency** due to quadrupod, subreflector.

Partial shadowing of the aperture by central sub-reflector and support structure (quadrupod):
(a) after reflection at the primary,
(b) before reflection at the primary. Projection of quadrupod onto the aperture of the primary.

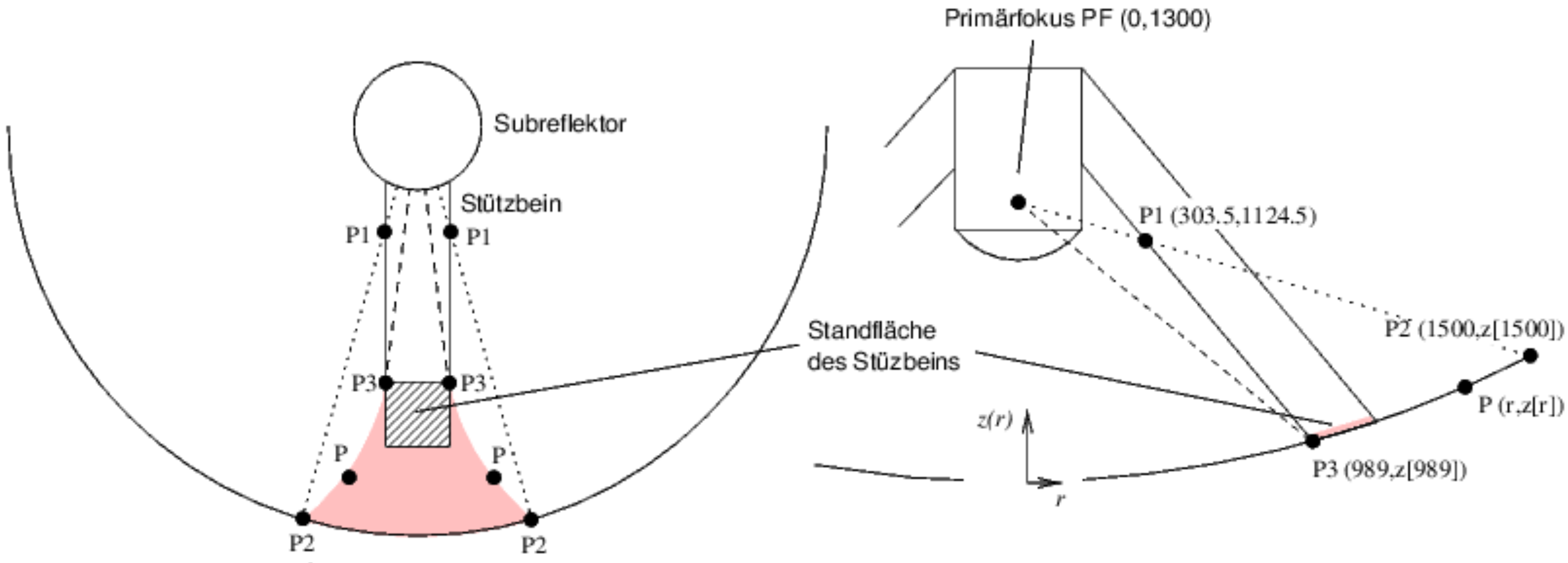

Abbildung 3.4: Von den Stützbeinen wird am Rand des Reflektors eine trapezförmige Fläche abgedeckt. Die Krümmung (in der Projektion auf die Ebene) der Strecke $\overline{P2P3}$ entsteht durch die paraboloide Gestalt des Hauptreflektors. Die gekrümmte Fläche kann durch ein gerades Trapez genähert werden. $z(r)$ ist in Abb. 3.3 aufgetragen.

(a) Blocked area caused by obstruction of the reflected spherical waves from the outside of the primary on their way to the primary focus. Here: KOSMA 3m telescope. Hiyama 1998 (Diplomarbeit, Univ. zu Koeln)

Aperture blocking of the 30m telescope Baars 2013

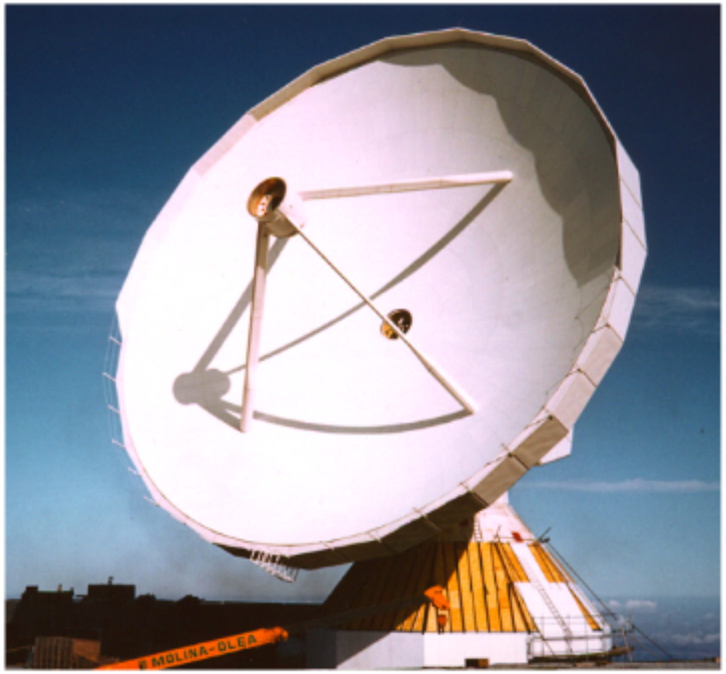

Name	M R T
Institute	IRAM (Spain)
Diameter (m)	30
Wavelength range (cm)	0.8 mm – 7 mm
Width of strutt (cm)	24 (60)
Illumination	Uniform / Tapered
Blocking percentage	**4.2 / 2.7**
Blocking Efficiency	**0.92 / 0.95**

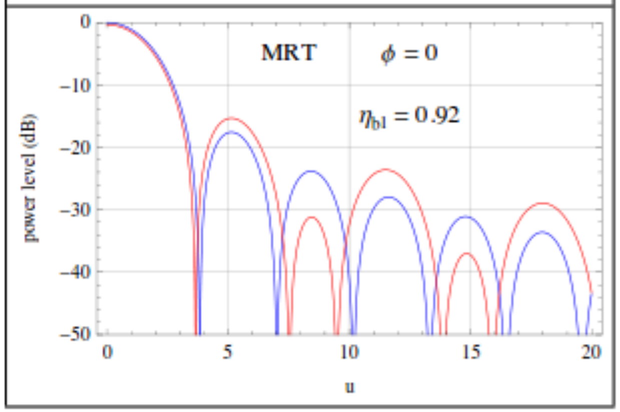

Blocking leads to a lowered aperture efficiency due to the decrease of the reflector area and the reduction of incoming energy available for reflection to the focus.

It also leads to an increase of the sidelobe level.

Some blocking efficiencies:
+ Effelsberg-100m: 0.85
+ IRAM-30m: 0.95
+ ALMA MT Mechatronics 12m: 0.97

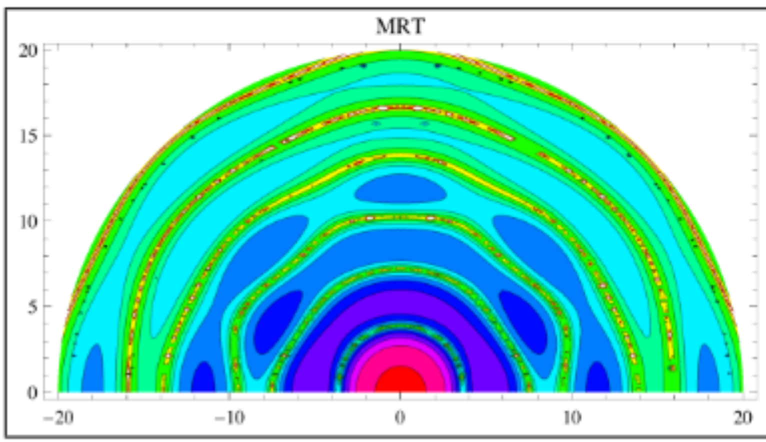

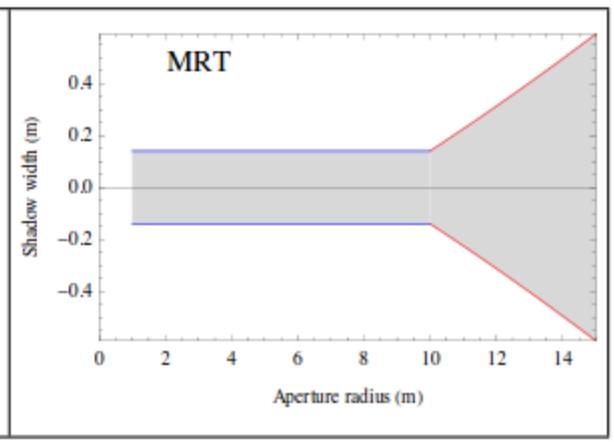

The homology design of this antenna incorporates the quadripod in the design of the reflector structure. This made it possible to move the penetration radius to a somewhat larger value than usual. On the other hand, the strong requirements on the stiffness and stability required the lower 1.4 m of the legs to have a larger cross-section. This is visible in the picture, taken during construction. The numbers given here result from an average value for entry into the calculation. A more precise calculation with the exact geometry decreases the blocking efficiency by one percent.

Aperture efficiency - surface errors

Product of all losses: $\eta_A = \eta_i \eta_s \eta_r \eta_e \eta_f \eta_b$

+ η_e = **surface error efficiency** ("Ruze loss", also called scattering efficiency)

Small scale, randomly distributed deviations of the reflector from the perfect paraboloidal shape cause phase errors over the aperture.
(Ruze 1952, Baars 1973, Baars 2007)

$\eta_e = \eta_A / \eta_{A0} = exp(-\sigma^2) = exp(-4 \pi \varepsilon / \lambda\ ^2)$

With the surface deviation ε, the root-mean-square phase error $\sigma = 4\pi\ \varepsilon/\lambda$ in radian, and the aperture efficiency for a paraboloid without surface error η_{A0} i.e. in the limit of long wavelengths.

Measured aperture efficiencies at the 30m

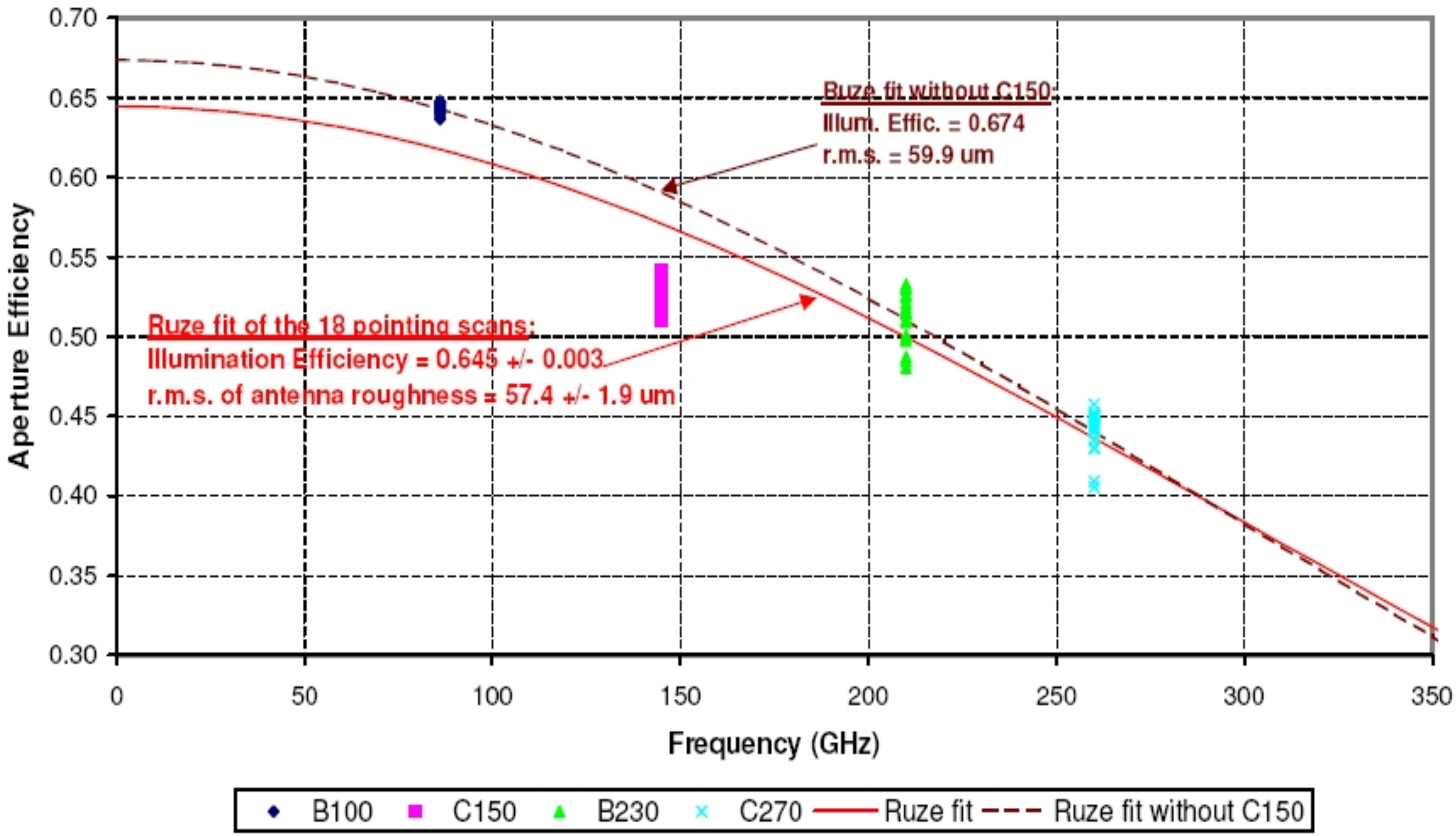

(measured by Juan Peñalver in August 2007)

Ruze's formula:
(ε = rms surface roughness)

$$\eta_A(\lambda) = \eta_{A0}\, e^{-\left(\frac{4\pi\epsilon}{\lambda}\right)^2}$$

Herschel: aperture efficiency: blocking and surface rms

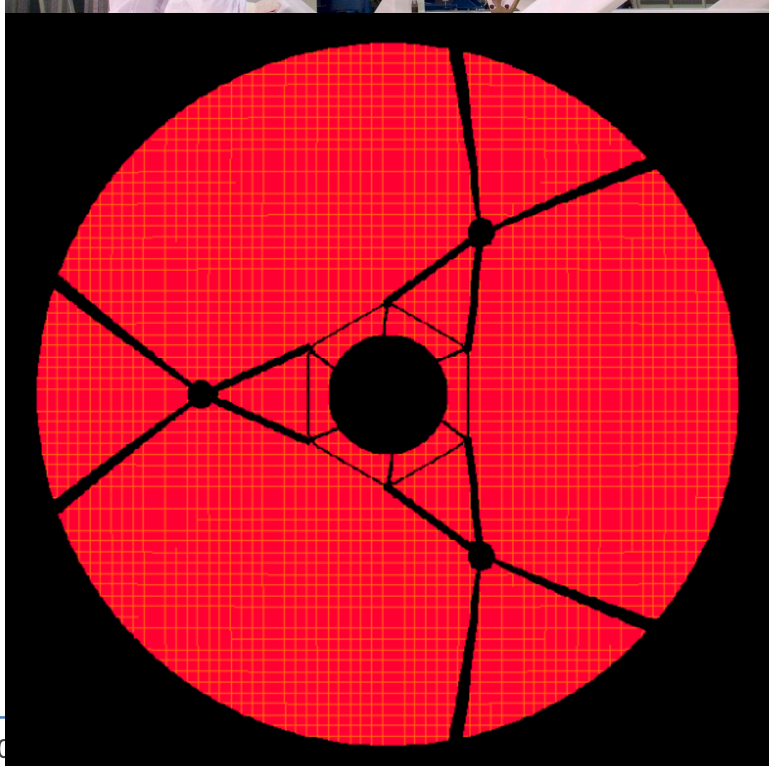

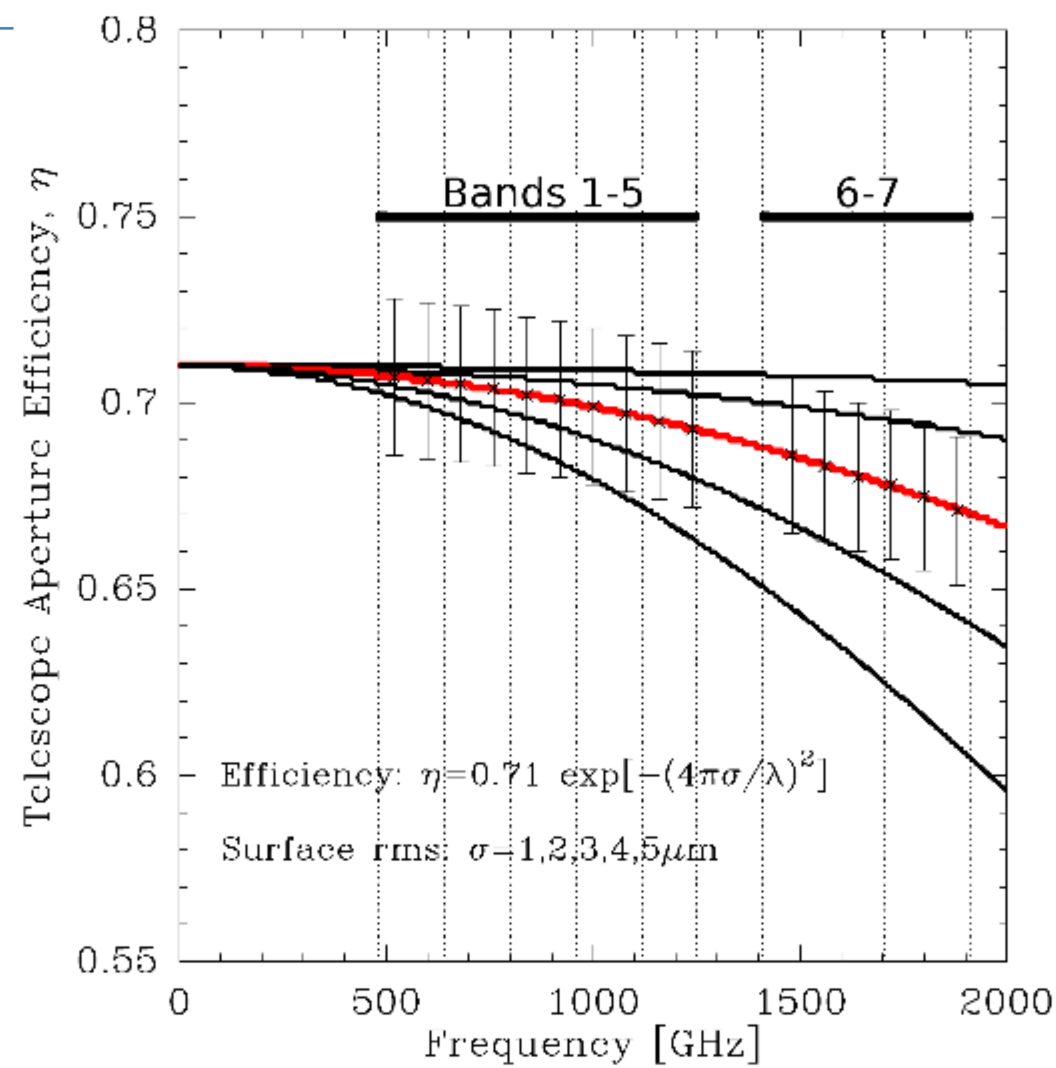

(Kramer 2006, HIFI Spatial Response Framework Document)

Aperture efficiency: elevation dependence

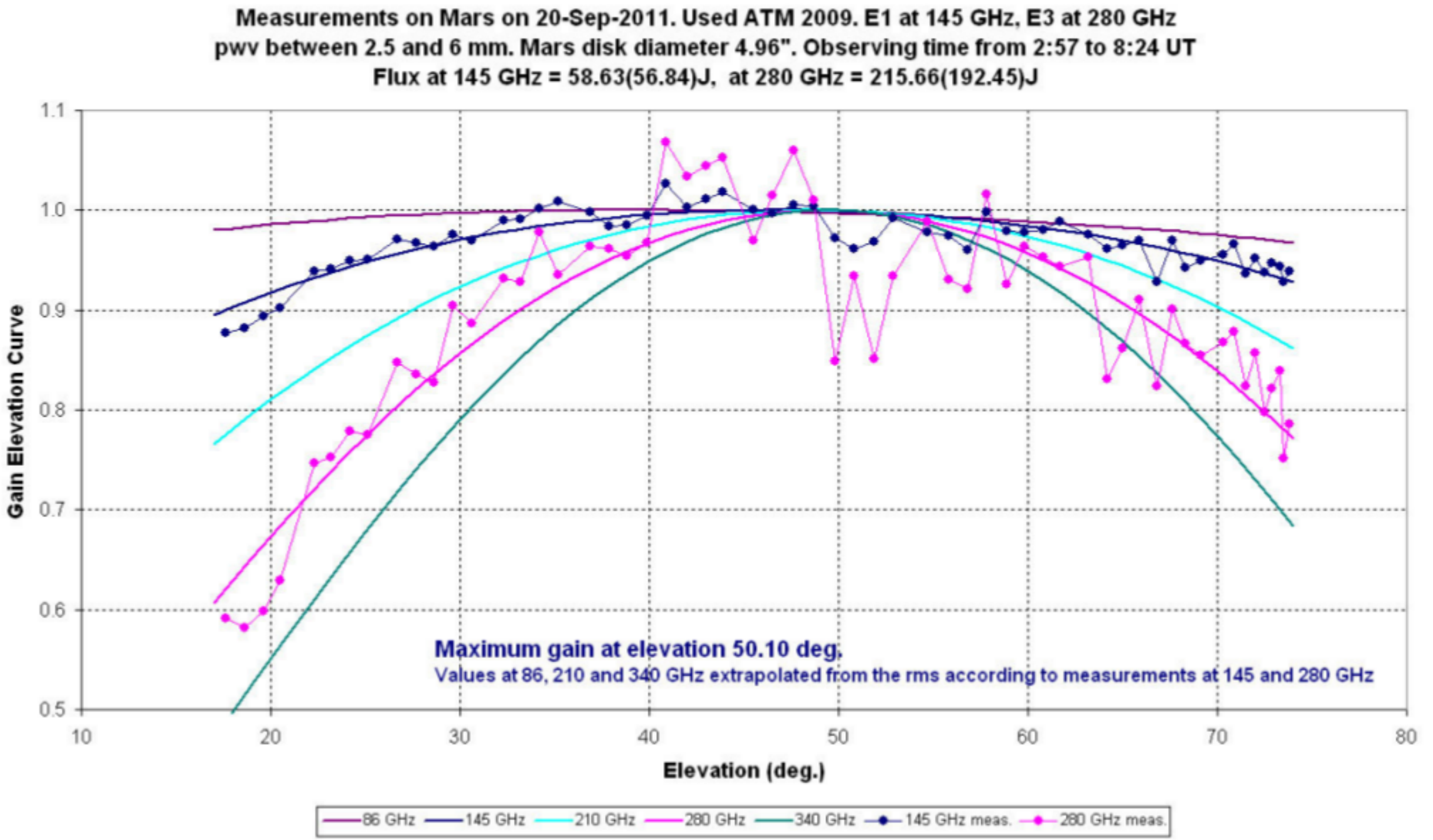

The 30m, like the 100m telescope, has a <u>homologous design</u>, i.e. the primary reflector maintains to a large degree its paraboloid shape, while the focus changes with elevation. The 100m Effelsberg telescope was the first with this design. More modern telescope have a stiffer design, but incorporating the same principle. Residual deviations cause, however, the <u>gain-elevation curve</u>.

Study to improve the surface accuracy of the 30m telescope

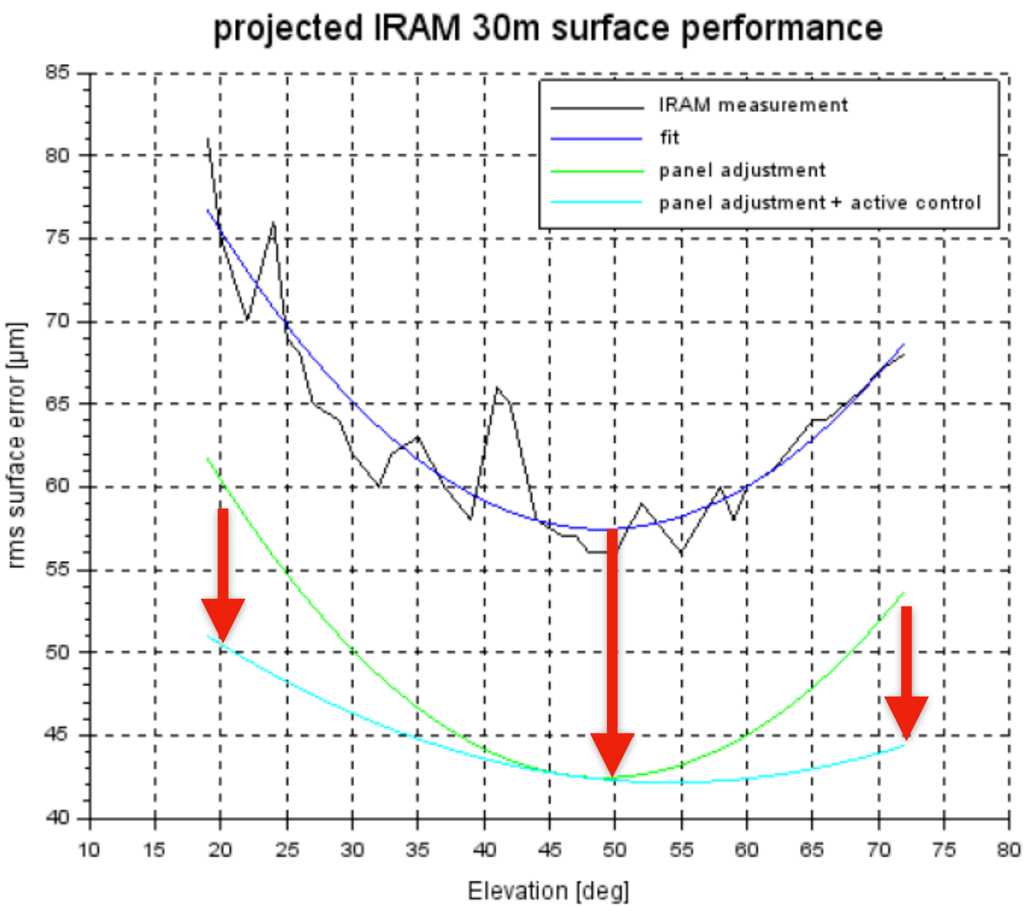

The pre-study indicates that the surface rms and the gain-elevation curve can be improved with two actions:

1/ dismounting and re-aligning all 420 panels on their 210 sub-frames. (At the same time, panel paint shall be replaced.)

2/ installing about 50-60 actuators, to use lookup-tables, to improve the gain-elevation curve.

Why upgrading the 30m ?

- Improved surface accuracy will
  - improve the beam efficiencies, sensitivities, calibration accuracy, and also
  - imaging quality in particular, beyond 200 GHz, and for low declination sources.
- Its first surface paint layer will be replaced.
- New servo and control system will improve
  - Slewing and tracking speeds to:
    - allow for more efficient observations of Galactic GMCs, and
      to better overcome atmospheric fluctuations for NIKA2 observations,
    - and to raise the elevation limit beyond 83°.
  - Reaction to wind will be improved, improving tracking performance, and losses of observing time due to high wind.
  - Implementation of new scanning patterns will be easier.

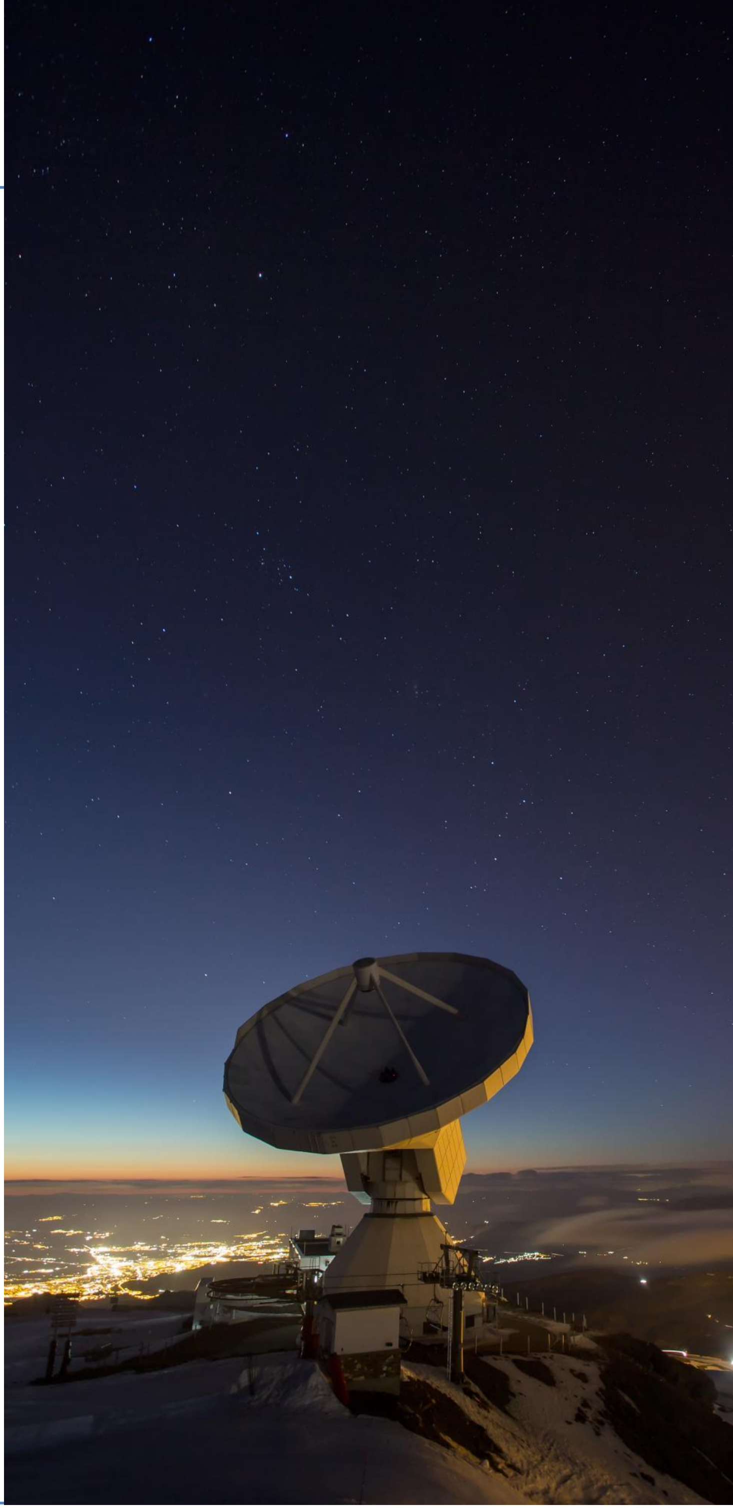

Extra transparencies:

Forward efficiency η_l

Widths of the main beam and the errorbeams

Fraction of power received through the forward hemisphere:

$$\eta_l = \frac{\Omega_{2\pi}}{\Omega_A}$$

The only way to estimate this efficiency is via skydips, by measuring the atmospheric emission with elevation (Airmass: A = 1/sin(El)).

$$T_A\,(El) = \eta_l T_{atm}\,(1 - e^{-tA}) + (1 - \eta_l)\;T_{amb}$$

$$T_A\,(El) = A - B\,e^{-tA}$$

Simple fit in p_plot_tip.mira

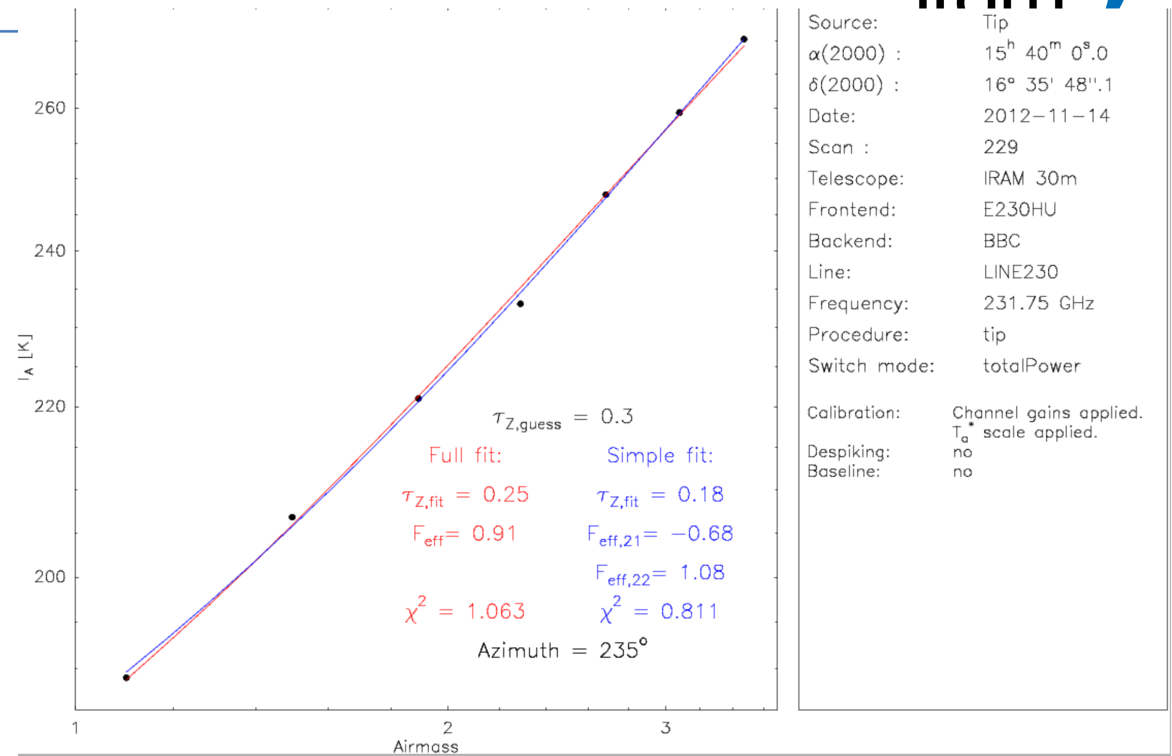

Remark:

- Skydips allow to measure the atmospheric opacity together with the forward efficiency.

The aim of astronomical observations is to obtain parameters of the emitting regions, like temperatures, densities, column densities, polarisation, time variability, etc.. To derive these quantities from the detected data, the properties of the receiving system have to be accurately known. In other words, the data have to be calibrated.

- Telescope
- Atmosphere
- Point spread function of the telescope
- Receivers: temperature, sideband gain ratio
- Antenna temperature and "Chopperwheel" calibration
- Telescope efficiencies: aperture, main beam, forward
- Stability and observing switching modes

based on:

- Lectures by ClemensThum at IRAM summerschool 2007
- Lecture by Pierre Hily-Blant at IRAM summerschool 2010
- Tom Wilson 2009: Introduction to Mm-Astronomy, Saas-Fe Lecture
- Jaap Baars 2007; The paraboloidal reflector antenna in radio astronomy, Springer
- **Tom Wilson et al.: Tools of Radio Astronomy, Springer**

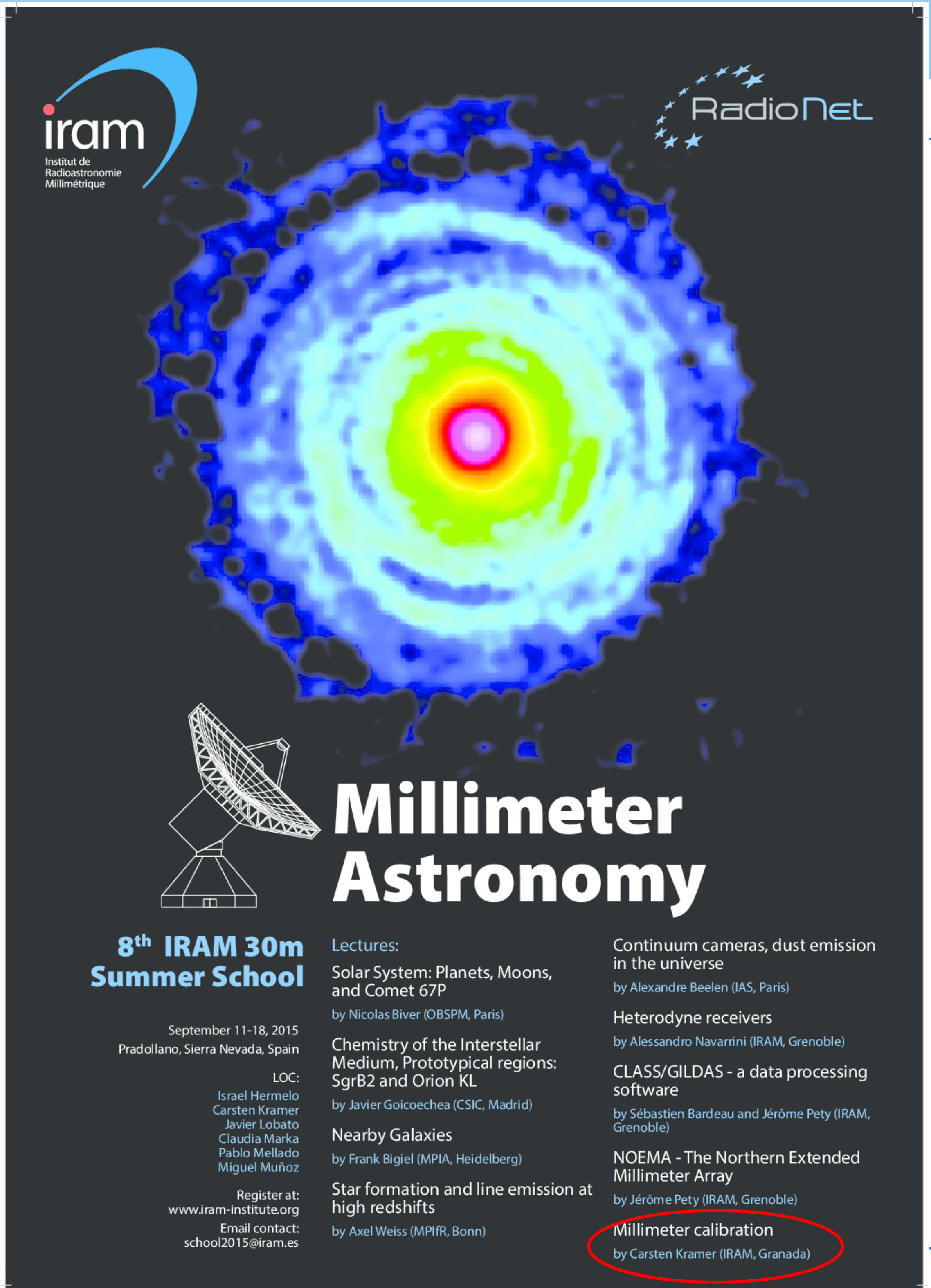

IRC+10216

Molecular shells surrounding the AGB star CW Leo at only 130pc distance.

^{12}CO 2-1 line at 230GHz mapped with HERA/30m by Cernicharo, Marcelino et al. 2014. Map size ~7'x7'.

Such stars provide ¾ of the matter returned to the interstellar medium.

The mass and chemical composition of their ejecta largely control the chemical evolution of galaxies.

Here, we can study the mass loss history over the past 8000 years.

The gas expands radially at 14.5 km/s. The typical shell separation is 1000 yr.

The mass loss rate is ~2 10^{-5} M_{sun} yr^{-1}.

The Galactic Center

2mm GISMO/30m (green)
250μm LABOCA/APEX (blue)
20cm VLA (red)

2mm emission tracing thermal dust emission of molecular clouds, but also free-free and synchrotron emission from ionized gas and non-thermal filaments.

Sources:

…,SgrB2, SgrB1, Radio Arc, Sickle, Arched Filaments, SgrA, SgrC, …

GISMO/30m observations:

Total observing time: 6.5hours.
NEFD ~ 9mJy sqrt(sec)
rms ~ 2-2.5 mJy
Dynamic range ~ 1000
(Staguhn et al. 2013 in prep.)

Equivalent paraboloid

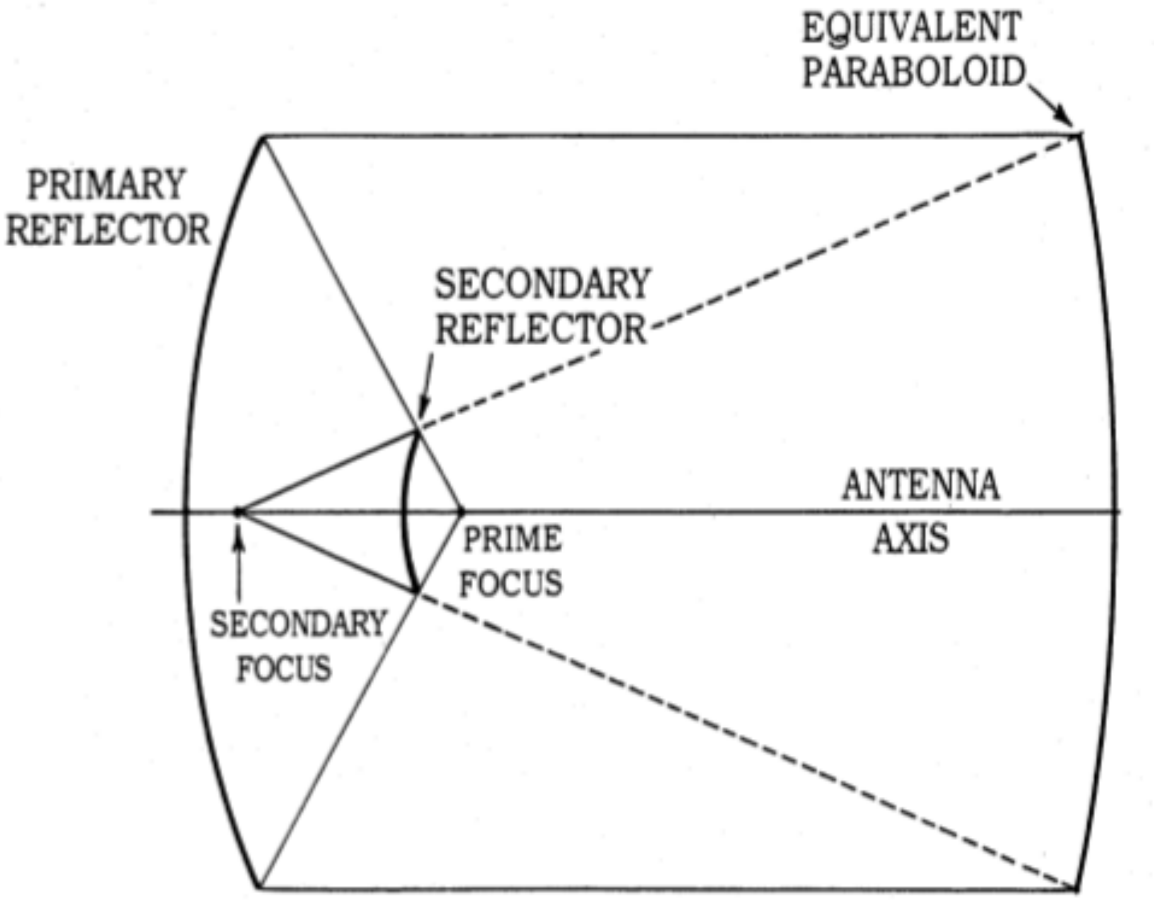

P.Goldsmith 1999

The equivalent paraboloid is the single reflector equivalent of whatever focussing system is employed.